Predictive Modeling of Laser Damage to Composite and Metallic Structures

a project presented to
The Faculty of the Department of Aerospace Engineering
San José State University

in partial fulfillment of the requirements for the degree
Master of Science in Aerospace Engineering

by

Tam Tran

February 2024

approved by

Dr. Maria Chierichetti
Faculty Advisor

ABSTRACT

Predictive Modeling of Laser Damage to Composite and Metallic Structures

Tam Tran

In this project, the possibility of developing an analytical model to predict laser damage onto a target surface will be explored, using physics to create a simple model that can predict the type and extent of damage. To perform more detailed analysis, a more complex finite element model of a laser is to be developed. Results between the two cases will be compared for metallic and composite materials.

ACKNOWLEDGEMENTS

I would like to acknowledge Dr. Maria Chierichetti for advising this project, as well as Dr. Nikos Mourtos and the Aerospace Engineering department at San Jose State University.

Table Of Contents

List of Figures

List of Tables

Symbols

Symbol	Definition	Units (SI)
η	Absorptivity Coefficient	-
P	Laser Power	W
C_P	Specific Heat	-
T	Temperature	K
V	Laser Scan Rate	Hz
q	Heat Flux	W/m^2
q_s	Surface Heat Flux	W/m^2
r	Laser Radius	m
ρ	Density	kg/m^3

1. Introduction

1.1 Motivation

The analysis of laser damage to composite structures can be valuable to various applications within the defense industry, notably involving the capability of using lasers in anti-missile defense systems. The application of lasers in air defense systems was previously limited to smaller aircraft, drones, and rockets, with these systems encountering issues with faster, more potent cruise missiles [1]. To improve existing applications of lasers for defense, development of more powerful lasers has been proposed. Understanding an empirical relationship between the strength of a laser and the geometry of the target can assist with the selection of laser power needed to cause structural failure, as not to waste additional resources. In addition to improving anti-air defense systems, understanding this relationship can aid in the design of missiles and aircraft structures that are more laser-resistant by understanding the threshold of power required to prevent failure.

Composite materials have started to be used in missiles due to lightweight characteristics and high performance in harsher weather conditions compared to metals [2]. The additional research on laser damage to composites in this project aims to improve existing systems by developing an analytical and numerical model that simulates the effects of laser damage on composite structures; the models will simulate the structural response for a variety of parameters that may be encountered by real-life defense systems.

1.2 Literature Review

1.2.1 Laser Systems and Damage

Directed energy systems, of which lasers are a classification, use electromagnetic energy as a defense mechanism to adversely affect aircraft, ranging from the disruption of electronics to the destruction of structures. Lasers are characterized by having a high concentration of energy and a monochromatic wavelength [3]. Within the broader category, lasers can be classified based on energy levels, with high-energy (greater than 10 KW of power) lasers being the most relevant in defense applications due to their effectiveness at causing structural damage to aircraft. High-energy lasers can be divided into further categories based on the type of gain medium. Chemical fuel-based lasers produce high energy but are less feasible in a realistic scenario due to the logistical challenges of maintaining volume and weight of the fuel. Solid-state lasers are easier to operate due to lower relative weight but produce less energy due to energy loss. Free electron lasers are an alternative option that produce high energy, but usage is limited due to large size.

When a target surface is impacted by a laser, the energy is only partially absorbed by the target, with a percentage of energy dissipating [3]. The absorptivity coefficient η of a material

represents the energy absorbed by the target relative to the energy output of the laser. For a flat melt surface, the absorptivity coefficient is given by [3]:

$$\eta = 0.7\left[1 + \exp\left(0.6\frac{\eta_m P}{(T_1 - T_0)\pi\rho C_p V r_0^2}\right)\right] \tag{1.1}$$

where η_m is the minimum absorptivity, P is the laser power, T_1 is the melting point of the target material, T_0 is the temperature at a point far away from the laser, ρ is the density of the material, C_P is the specific heat of the material, V is the scan rate of the laser, and r_0 is the radius of the laser. As the absorptivity coefficient varies, it must be calculated on a case-by-case basis.

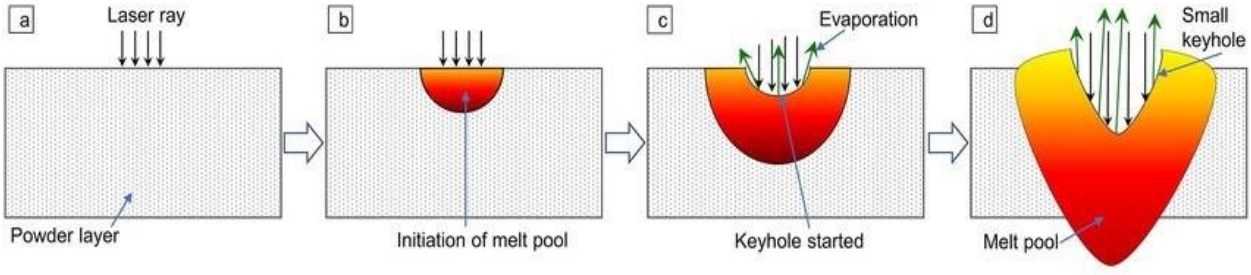

Figure 1.1: Damage formation from laser impact [4].

Damage from lasers' effects encompasses a variety of damage types, with damage resulting from a combination of multiple damage types, such as melting, heating, and vaporization.

Melting occurs when the temperature of the target reaches the melting point of the target material [3]. To cause structural damage, the laser creates a hole in the target, in which molten material is removed and exposes new material to the laser. The melt pool, defined as the area of molten material created by the laser, is the result of a change in the target surface's geometry as molten material is removed [5]. The absorptivity of a target surface can increase from reflective effects from a change in the geometry of the melt pool. For military applications, in which exposure time to a laser can be limited, melting alone is generally not enough to cause significant damage.

Heating occurs when the target surface absorbs energy from the laser as thermal energy. Energy on the surface propagates throughout the rest of the material in the normal direction to the target surface due to the electron gradient being the highest in that direction [6]. For applications with thin target surfaces, heat would then propagate in the direction parallel to the target surface. The rate of propagation depends on the thermal diffusivity of the target material and time of exposure to the laser. However, heating is generally not enough to cause significant structural damage on its own, with an exception for cases in which the target surface is soft [3].

Vaporization is another form of damage that occurs in high energy lasers, where damage is the resultant of the conversion of the target surface to a gaseous state [3]. During this process, escaped metal vapor from the target deforms the target surface through reactive forces, which push back against the target surface to cause a keyhole deformation [7]. To cause significant damage, molten material from melting must be removed through vaporization. Thus, the rate of heat

vaporization must be greater than the rate of erosion of the target surface due to melting for vaporization to cause damage. Vaporization loss is dependent on the material of the target surface.

Vaporization is the most relevant type of damage when considering laser damage in military applications, as the fast-moving nature of the targets limits the amount of exposure time from the laser. Comparatively, heating and melting are not as effective as vaporization in terms of causing structural failure; thus, the model for thermal damage will focus on damage from vaporization.

1.2.2 Thermal Conductivity Approach

A possible approach to assessing damage is through thermal conductivity of the target surface. Lazov et al. use the thermal conductivity equation [8]:

$$C_P \frac{dT}{dt} = div(k\ grad\ T) + q_s(1 - R)\alpha \tag{1.2}$$

where q_s is surface power density, R is the reflection coefficient, α is the absorption coefficient, k is the thermal conductivity coefficient, c is the specific heat capacity, ρ is the density, and T is the temperature. Absorption occurs in the outer layer of the surface, resulting in a heat source being created [8]. The heat source is then absorbed by the rest of the source by thermal conduction. Lazov et al. note that the thermal conductivity equation is likely too complex to solve analytically, but that it can be solved using a finite element or Multiphysics approach. The thermal conductivity approach to modelling laser damage states that damage occurs when the temperature of the target exceeds the vaporization temperature of the target material, ablation occurs [9]. The prediction of damage in this model is straightforward but does not account for the dimensions of the laser.

Li et al. examine the usage of a Gaussian heat model to predict thermal conductivity, with the following equation used to describe the Gaussian heat source [10]:

$$q(x, y) = \frac{\eta Q}{2\pi r^2} \exp\left(\frac{x^2 + y^2}{2r^2}\right) \tag{1.3}$$

where q is the density of heat flux at a given coordinate (x, y) looking at the target surface, η is the absorptivity coefficient, Q is the output of the laser, and r is the radius of the laser. The Gaussian distribution model is assumed to be circularly symmetrical. Using the assumption that temperature is linearly distributed in one conductive direction, the two-dimensional shape of the deformation can be given by [10]:

$$f(x) = h \cdot \exp\left(\frac{-x^2}{(.5r)^2}\right) \tag{1.4}$$

where h is the distance between the location of maximum deformation and the height of the original target surface, x is the distance from the center of deformation to the furthest point where deformation occurs, and r is the radius of the laser. The equation for the shape of the target surface damage is useful for a prediction of damage while missing information on one of the parameters, such as being able to find the depth of damage from the radius that the damage occurs at with respect to the laser. The Gaussian representation of the laser for the thermal conductivity method allows the model to be tuned for laser size and parameters.

Fu et al. use the Gaussian heat model in a finite element analysis of the interaction between a laser with changing position and metal powder bed. In this model, the position of the laser varies over time. The representation of the heat source movement is shown in Figure 1.1:

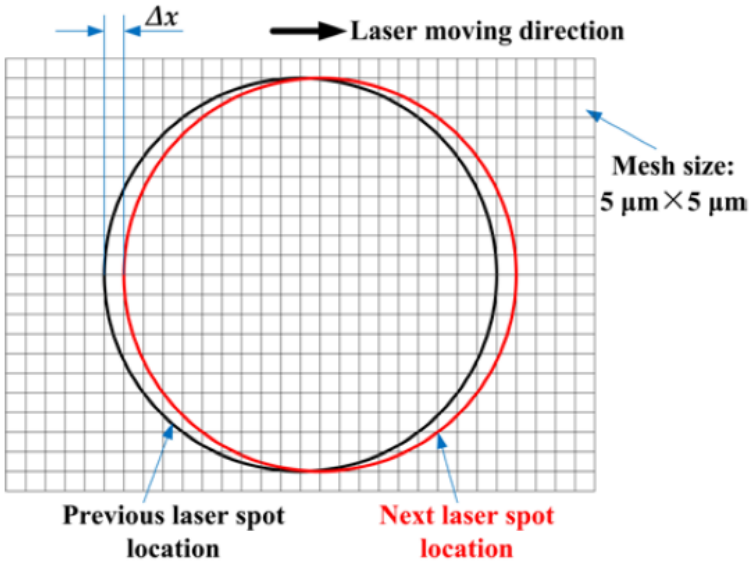

Figure 1.2: Representation of laser source movement [11].

where Δx is the change of position of the laser. The heat input over a defined time step can be obtained through a space integration of the Gaussian heat source equation [11]. The total heat input from the laser source over a time interval is found by summing the inputs of the individual mesh elements. The damage to a given target surface can be determined based on variable factors of irradiation time, laser power, and temperature. This study creates a predictive model for metal powder materials, but the heat conductivity approach should still be valid for composite materials, albeit with different material properties. Accounting for a moving laser is essential to recreating a realistic scenario of laser-target applications in defense, as laser tracking will never be perfect.

Zigunov created a simplified model of temperature distribution after laser exposure to a target in MATLAB as shown in Figure 1.3 [9]:

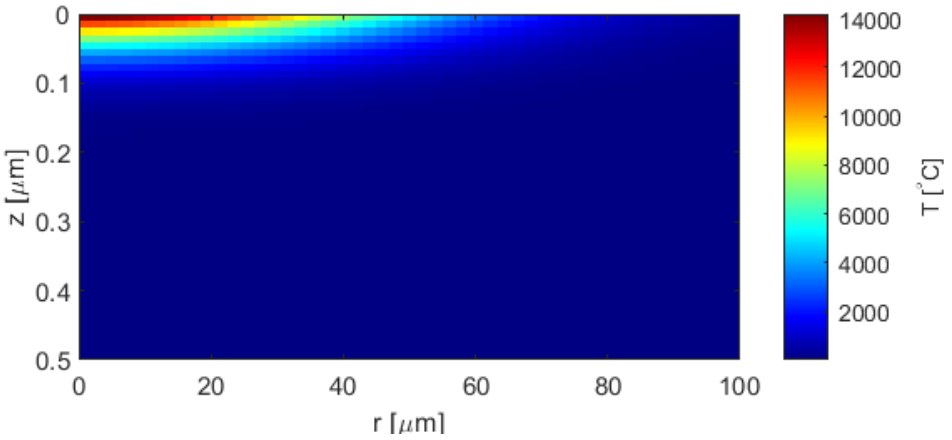

Figure 1.3: Temperature of the target surface after laser exposure [9].

where *r* is the distance away from the center of the laser and *z* is the depth of the target, with the zero-distance representing the target surface. Zigunov uses the two-dimensional heat equation with a Gaussian heat source as a basis for the equation [9]. Zigunov uses constant properties for diffusion and conductivity in the approximation but note that property curves can be defined to more accurately simulate temperature distribution. The temperature distribution is a three-dimensional problem, but assuming the laser to be a Gaussian heat source in cylindrical coordinates allows the problem to be simplified into a two-dimensional model. The behavior of damage does not change with respect to the orientation angle; thus, the damage can be represented as a function of depth and radius.

For this study, a two-dimensional model comparing depth and radius will be created using the Gaussian heat source assumption for a stable laser. The damage will be assessed through thermal conductivity, where structural damage is achieved for temperatures that exceed the vaporization temperature. This model will then be adjusted for a moving laser.

1.2.3 Material Properties

To understand the extent of damage on a target surface, the material properties must be studied. For the purpose of this study, the material properties of both composite materials and metals will be studied to understand the differences in response.

For thermal damage to occur via vaporization, the heat of the target must exceed the heat of vaporization. For carbon fiber, the heat of vaporization is 128 K-Cal/gm, which occurs at 4612 degrees Celsius [12]. The melting point of carbon fiber occurs from 3652 to 3697 degrees Celsius.

As the absorptivity coefficient of a material varies with the properties of the laser and the material properties of the target, the absorptivity needs to be calculated for a unique combination of material and laser. Cook et al. state that absorptivity decreases with increasing wavelength, stating that the angle of incidence also affects absorptivity [13]. Boley et al. experimentally determine the absorptivity coefficients for carbon fiber and a laser of varying wavelength for p-waves and s-waves, as shown in Table 1.1 [14]:

Table 1.1: Absorptivity for varying wavelength lasers for carbon fiber [14].

Wavelength (μm)	Absorptivity (s)	Absorptivity (p)
0.53	0.90	0.91
0.8	0.87	0.88
1.06	0.86	0.88
1.3	0.84	0.86
2.0	0.80	0.83
2.8	0.77	0.81
3.8	0.74	0.79

The experimentally found values for the absorptivity coefficient of carbon fiber match the hypothesis that Cook et al. state.

Alsaddah et al. experimentally determined the absorptivity coefficients in terms of percentage for Ti6Al4V, AlSi12 and Cu, which are all metals or metallic alloys, shown in Figure 1.4 [15]:

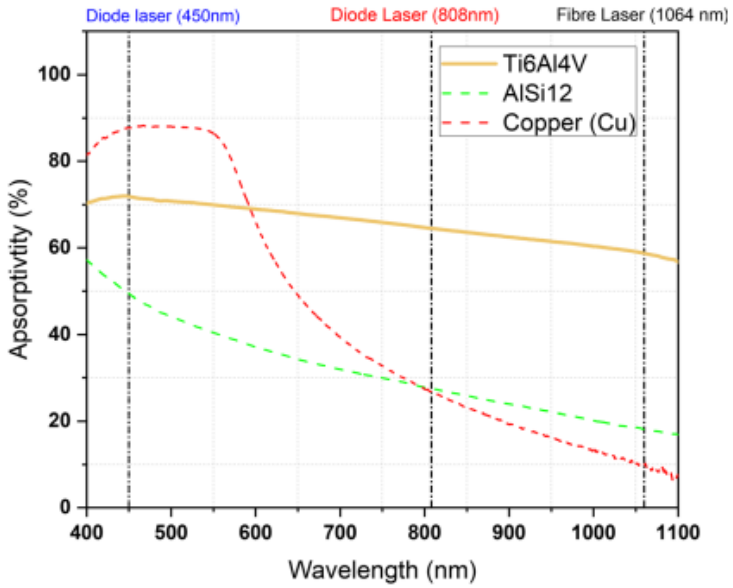

Figure 1.4: Absorptivity vs wavelength for Ti6Al4V, AlSi12 and Cu [15].

All three materials exhibit a general decrease in absorptivity, although copper has a slight increase in absorptivity for lasers with a wavelength of approximately 400 to 550 nanometers.

In flight, a missile already undergoes thermal stress before the application of a laser. These values can be added to the temperature that results from laser heating until the minimum temperature for vaporization is achieved. The temperatures for a missile flying at Mach 4 are given in Table 1.2 [16]:

Table 1.2: Temperatures for missile components at Mach 4, Fahrenheit [16].

Radome	1500
Nose tip and unswept leading edges	1550
Swept leading edges	1475-1520
Forebody skin and control surfaces	1460-1480
Aft body skin	1275-1300
Subsonic inlet ducts	1600
Supersonic inlet ducts	1470
Gas generator	4600
Combustor	3660
Nozzle	3500

1.3 Proposal

The objective of this project is to study the laser-target interaction for composite materials and develop a finite element model to predict damage and failure behavior from the impact of a laser on metal and composite surfaces.

1.4 Methodology

To understand the physics behind the damage caused to composite structures by a laser, a literature review must be performed. The possibility of developing an analytical model to predict damage will be explored, using physics to create a simple model that can predict the type and extent of damage. To perform more detailed analysis, a more complex working model of a laser is to be developed. A variety of parameters will be selected based on prior studies, including the type and characteristics of the laser, the material and characteristics of the target surface, geometry, and the flight and exposure conditions of the laser with respect to the missile. The feasibility of performing a finite element analysis using ANSYS to accurately model the thermal effects of laser damage to a composite model will be determined through a literature review of similar works. In the case that a finite element approach is unsatisfactory, a Multiphysics model can be attempted, in which the necessary software to perform one must be determined.

Following the establishment of an analytical and complex model, the two cases will be compared, including to determine if an analytical model can be used to predict damage with a similar result to the more complex model. Following the comparison, it can be determined that either the analytical model, the complex model, or both are sufficient as an accurate estimation of laser damage to composite structures.

2. Heat Diffusion Model using the Finite Difference Method

2.1 Finite Difference Method

The finite difference method is a method of numerically solving differential equations using approximations for the derivatives. The finite difference method partitions a differential equation into time and space, which is then solved by approximation at equally spaced points [17]. Thus, the relation between the time derivative and space derivative can be used to solve the thermal diffusion equation. Zeneli et al. use a forward difference version of the finite difference method to estimate the behavior for solid-liquid phase changes in metals, which gives the following recurrence equation [18]:

$$\rho C_P {T_i}^{j-1} \frac{{T_i}^{j} - {T_i}^{j-1}}{\Delta t} = k \frac{T_{i+1}^{j} - 2{T_i}^{j} + T_{i-1}^{j}}{\Delta x^2} \tag{2.1}$$

where ρ is the material density, C_P is the coefficient of pressure, T is the temperature, t is the time, and x is space. The left side of the equation represents a forward difference time derivative at time t_j, whereas the right side of the equation represents a central difference at position x_i. The backwards difference version of Eq. 2.1 can be expressed as follows:

$$\rho C_P {T_i}^{j} \frac{T_i^{j+1} - T_i^{j}}{\Delta t} = \frac{T_{i+1}^{j+1} - T_i^{j+1} + T_{i-1}^{j+1}}{\Delta x^2} \tag{2.2}$$

Both the forward and backward difference methods can be used to solve for heat diffusion, although each case will result in a different error. The forward difference gives a better estimate at values closer to the first grid point, whereas the backwards difference gives a better estimate at values closer to the final grid point. For the purpose of this study, a forward difference version of the finite difference method will be used, as the damage is most relevant in the local area of the laser impact. A visual representation of the difference between the forward and backward difference methods is shown in Fig 2.1 [19].

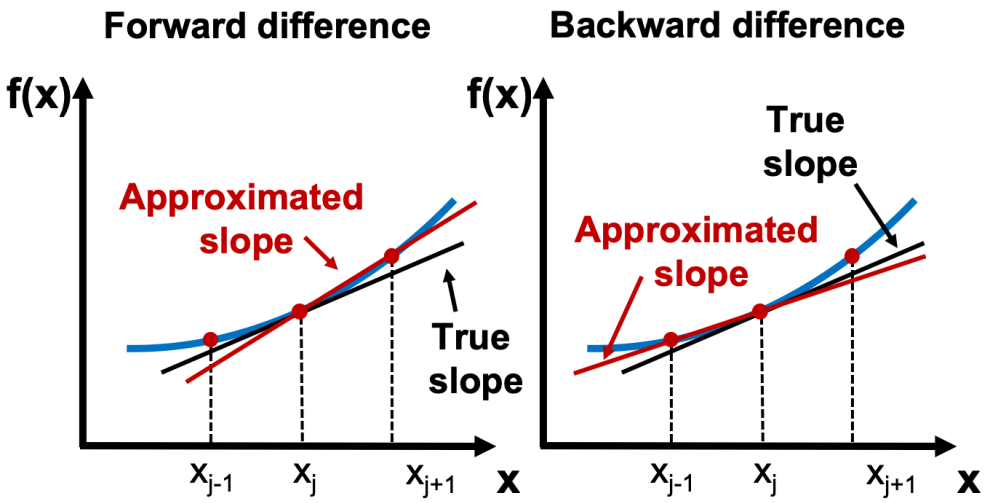

Figure 2.1: Visual representations of forward and backward difference [19].

To solve a differential equation using recurrence, the boundary conditions and initial conditions must be defined. Thus, the temperature at must be defined for the first and last values of *i* and the first value of *j*. These values can be determined on a case-by-case basis dependent on accepted measured values for inflight conditions.

The finite difference method is relatively simple and provides accurate results in cases with simple geometry, but the approximation loses accuracy with increasing complexity in the geometry [17]. The finite difference method requires a structured grid for the discretization of space due to the recursive nature of its calculations. A non-uniform grid can be created depending on geometry but might not be required for laser damage applications due to the relatively small laser size with respect to the rest of the intended target and the subsequent localization of the damage.

Note that the size of the elements of the grid can be reduced to increase accuracy, but the computational power of MATLAB restricts the number of elements used due to computation time. Given that the laser impulse occurs over an extremely short period of time, a limitation must be placed on a case-by-case basis when discretizing the space derivative.

2.2 Methodology for a Finite Difference Model of Thermal Diffusion

A finite difference model was created to solve the thermal diffusion problem resulting from a laser impact. This model estimates the temperature distribution throughout the material with respect to time after exposure to the laser. In this model, the target surface is assumed to have been impacted by a laser for a defined period of time, where the material heats and temperatures increase. The heat diffusion within the material is studied in the time immediately after the impact, estimating the amount of time it would take for significant damage to occur. The temperature distribution is represented as the distance away from the initial impact location, which simplifies temperature distribution into a one-dimensional representation. A maximum temperature threshold

is set based on the vaporization temperature of the target material, where it is assumed that all regions where the temperature exceeds the vaporization temperature of the materials will vaporize.

The laser ablation simulation created by Zigunov is a quick and effective way of estimating the temperature distribution for a laser impact on a target material, but it has a few drawbacks that prevent it from being used on its own for analyzing laser damage in aerospace applications. Firstly, the simulation measures damage in a very localized area with respect to depth and horizontal distance from the location of impact. In addition, the simulation only measures the temperature change during the laser impact but cannot measure the temperature distribution due to heat diffusion in the time following the laser impact. However, the laser ablation simulation is still useful for its ability to calculate the temperature distribution immediately after the laser impact, thus allowing it to be used in conjunction with the finite difference model of thermal diffusion to estimate the temperature distribution in the seconds after the impact.

Using input parameters for a given scenario, the Zigunov laser ablation simulation can be run to determine the temperature at the location of impact. The temperature at the point of impact found in the laser ablation can be used as a boundary condition for the heat diffusion model, with all grid elements making direct contact with the laser having that temperature at the beginning of the simulation. The surface opposite the impacted surface has a boundary condition with the initial temperature before impact, which is a combination of the air temperature and the added temperature midflight from Figure 1.5. The finite difference method is then applied to determine the temperature distribution throughout the grid for each time interval, resulting in a temperature versus time graph. Figure 2.2 shows a simplified general model for the initial temperature conditions for heat diffusion, where the red grid elements have an input temperature from the laser ablation simulation and the blue grid elements are the environment temperature.

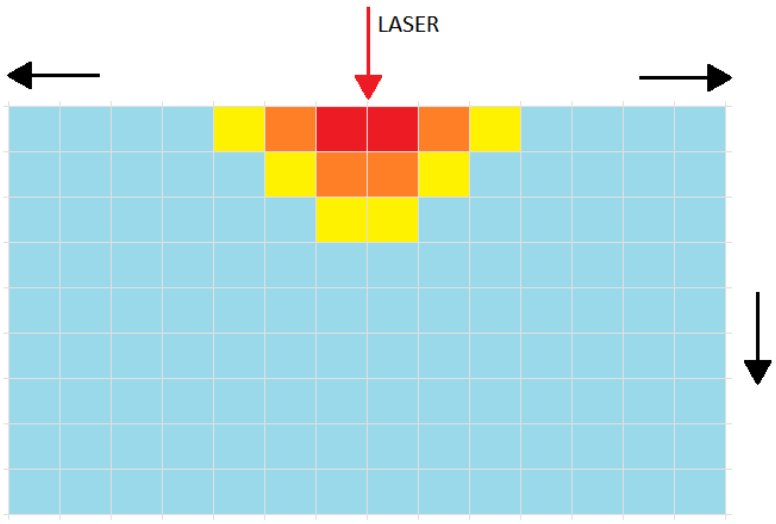

Figure 2.2: Heat diffusion initial temperature conditions example, general case

The initial condition depends on the size of the mesh and the size of the mesh elements. A constant temperature value must be chosen to represent each grid based on the temperatures found

in the laser ablation simulation. For this model, the highest temperatures found in each grid based on the laser ablation simulation was chosen as the representative initial temperature. Although this might lead to an overestimation for the heat diffusion, the error would not be too significant in a forward difference model until a high number of time steps, where the behavior of the heat diffusion usually stabilizes within a lower number of time steps with constant initial and boundary conditions.

2.3 Heat Diffusion Model Cases

2.3.1 50-kW Laser, Carbon Fiber

To determine the boundary conditions for the impacted surface, Zigunov's laser ablation simulation was run with modified inputs for the scenario. The laser properties are given in Table 2.1.

Table 2.1: Laser properties, Case 1

Laser Pulse Energy	Focal Radius	Pulse Time
50 mJ	0.5 mm	100 ns

In addition, the energy density of the laser in terms of Joules per square centimeter can be found using the following equation [9]:

$$energy\ density\ =\ \frac{pulse\ energy}{\pi(focal\ radius)^2} \times 10^{-4} \tag{2.3}$$

Using this formula, the energy density of the laser used in this case is equal to 6.366 Joules per square centimeter.

In addition to the laser properties, the original laser ablation simulation was modified for a change in material properties. The material properties for titanium are provided in Table 2.2.

Table 2.2: Carbon fiber material properties

Absorptivity	Thermal Conductivity	Density	Heat Capacity
0.87	1000 $\frac{W}{m \cdot K}$	1750 $\frac{kg}{m^3}$	2.02 $\frac{kJ}{kg \cdot K}$

The laser ablation simulation was performed using the inputs in Tables 2.1 and 2.2. The graphical result of the simulation is given in Figure 2.3 [16].

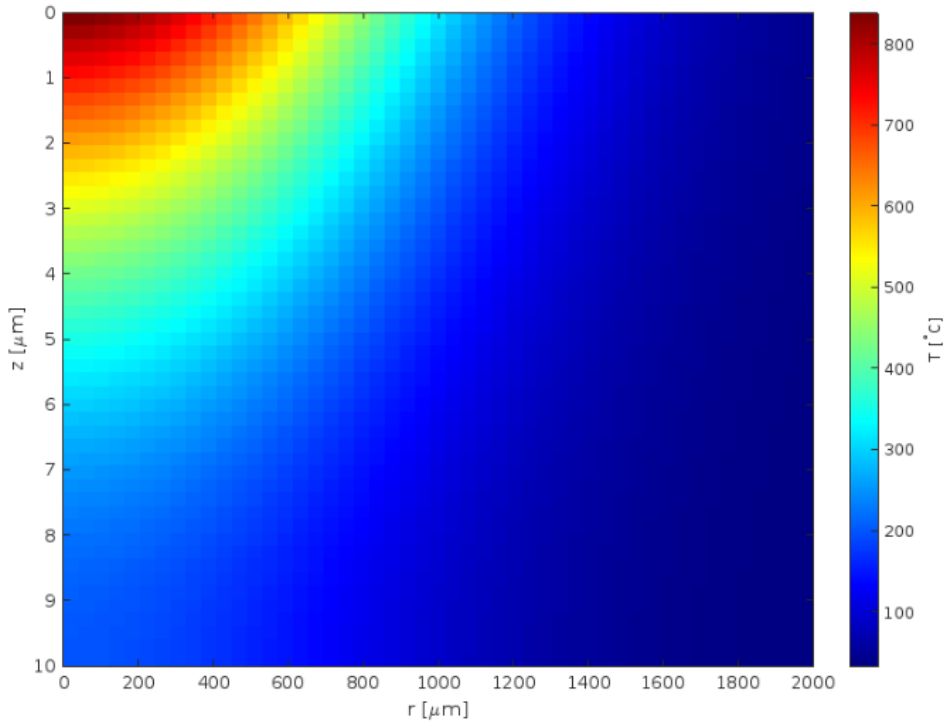

Figure 2.3: Temperature distribution of Zigunov's laser ablation simulation [9].

The maximum temperature occurs at the grid point closest to the laser impact. For this case, the grid elements have a height of one micrometer and a width of 0.5 millimeters, equal to the focal radius. The approximation for the initial conditions used are shown in Figure 2.4.

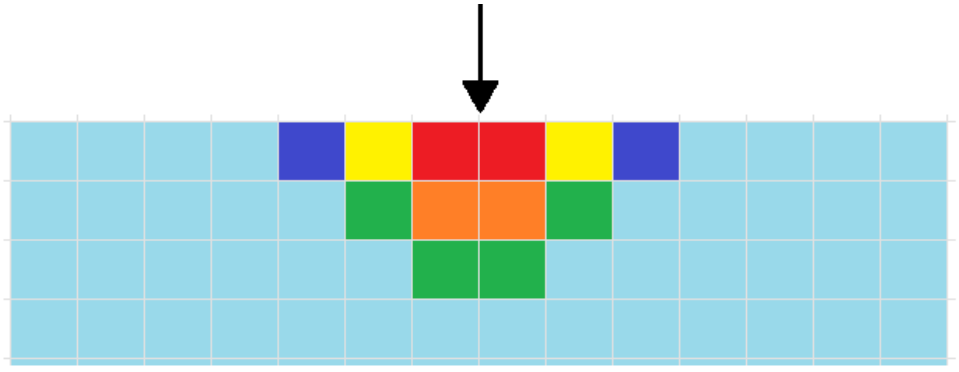

Figure 2.4: Local initial condition grid, Case 1.

For clarification, the associated temperature values for each grid color are given in Table 2.3:

Table 2.3: Initial conditions color map, K

Red	Orange	Yellow	Green	Blue
1112 K	980 K	887 K	765 K	565 K

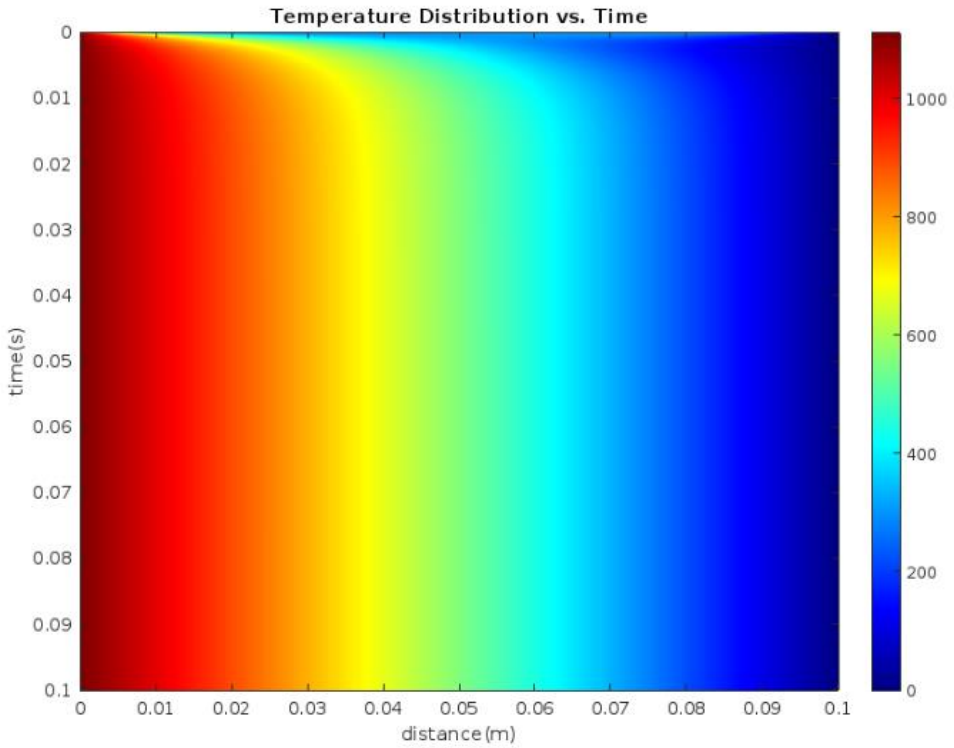

Figure 2.5: Heat diffusion temperature distribution with respect to time

The maximum temperature in this model is only 1112 K, short of the 3652 K melting temperature and 4885 K vaporization temperature of carbon fiber. However, the epoxy layers within the carbon fiber layup will undergo damage within this temperature threshold. While the carbon fiber may not vaporize or melt, structural damage will still occur as a result of delamination from the failure of the epoxy layers.

2.3.2 50-kW Laser, Titanium

A case was performed with parameters simulating a 50-kW, 808 nm wavelength diode laser impacting a 0.1 m thick sheet of titanium, intended to represent the target material of a F-16.

The Zigunov laser ablation simulation was performed with the following laser and material properties:

Table 2.4: Laser properties, Case 2

Laser Pulse Energy	Focal Radius	Pulse Time
50 mJ	0.5 mm	100 ns

Using Eq. 2.3, the energy density of this laser is equal to 6.366 Joules per square centimeter. The material properties of titanium inputted into the simulation are given in Table 2.5:

Table 2.5: Titanium material properties

Absorptivity	Thermal Conductivity	Density	Heat Capacity
0.63	$11.4\frac{W}{m\cdot K}$	$4420\frac{kg}{m^3}$	$130\frac{kJ}{kg\cdot K}$

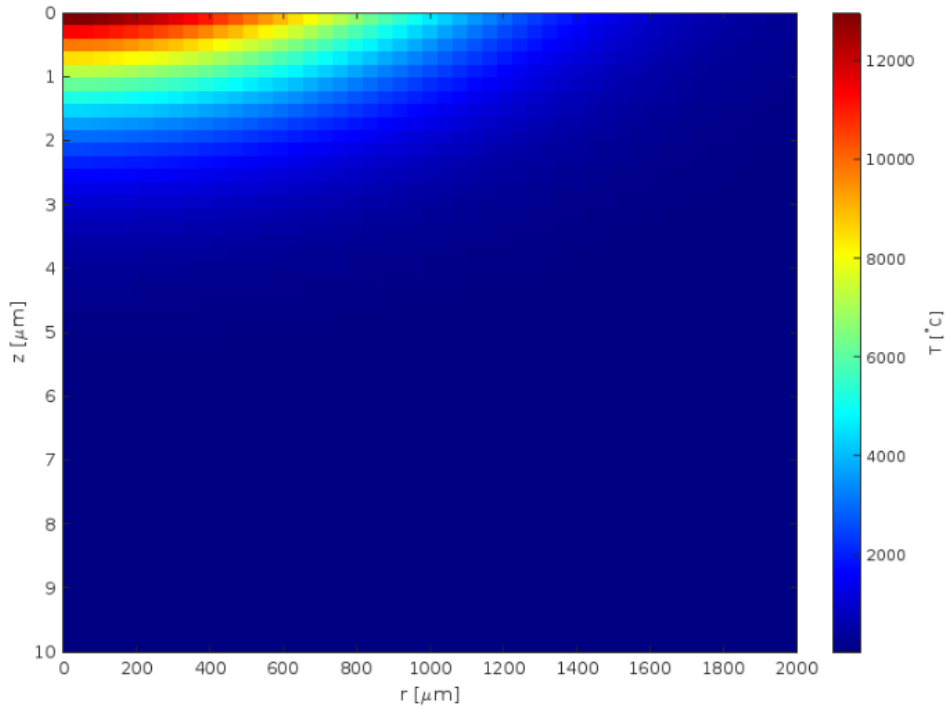

Figure 2.6: Temperature distribution of Zigunov's laser ablation simulation [9].

The maximum temperature found in the Zigunov laser ablation simulation for this case is 13238 K. For this case, the grid elements have a height of one micrometer and a width of 0.5 millimeters, equal to the focal radius. The initial condition grid is approximated as shown in Figure 2.7:

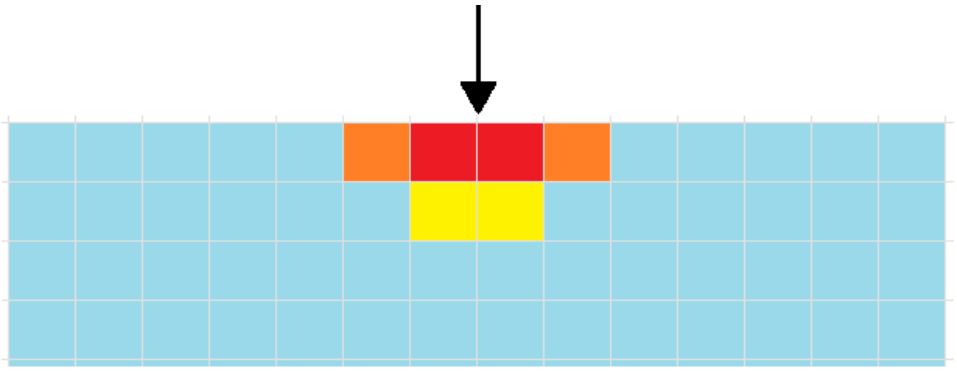

Figure 2.7: Local initial condition grid, Case 2

where the red grid elements have a temperature of 13238 K, the orange grid elements have a temperature of 10301 K, and the yellow grid elements have a temperature of 6441 K. The temperature distribution in terms of depth with respect to time is given in Figure 2.8:

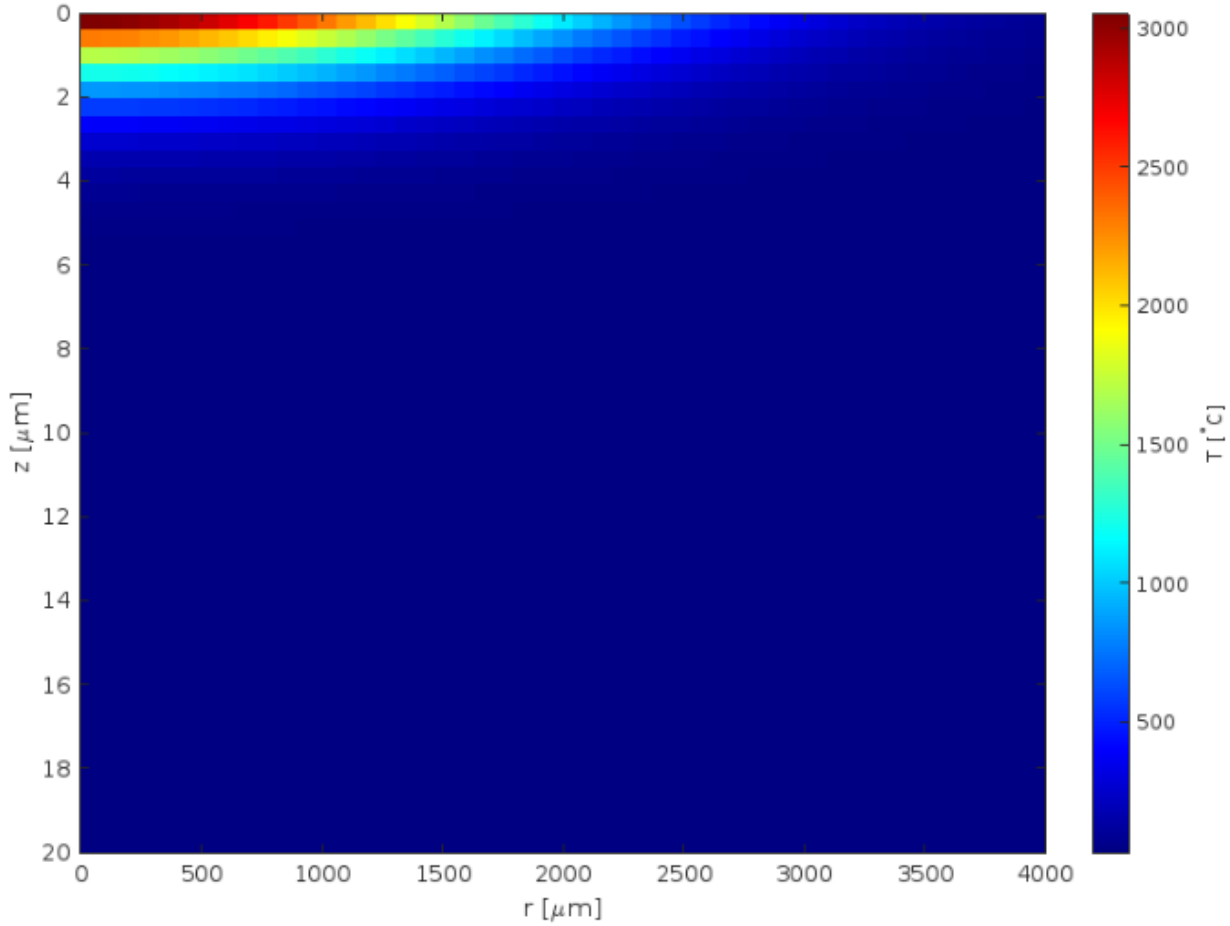

Figure 2.8: Temperature distribution versus time

The heat diffusion model results in a spectrum of values from the initial temperature of the scenario to the maximum temperature from the laser ablation simulation. The vaporization

temperature of titanium lies within the spectrum at 2023 K. It can be assumed that all grid elements with a temperature greater than the vaporization temperature will vaporize, thus being physically removed from the target surface. The model can be adjusted to exclude all values above the vaporization temperature, as shown in Figure 2.9:

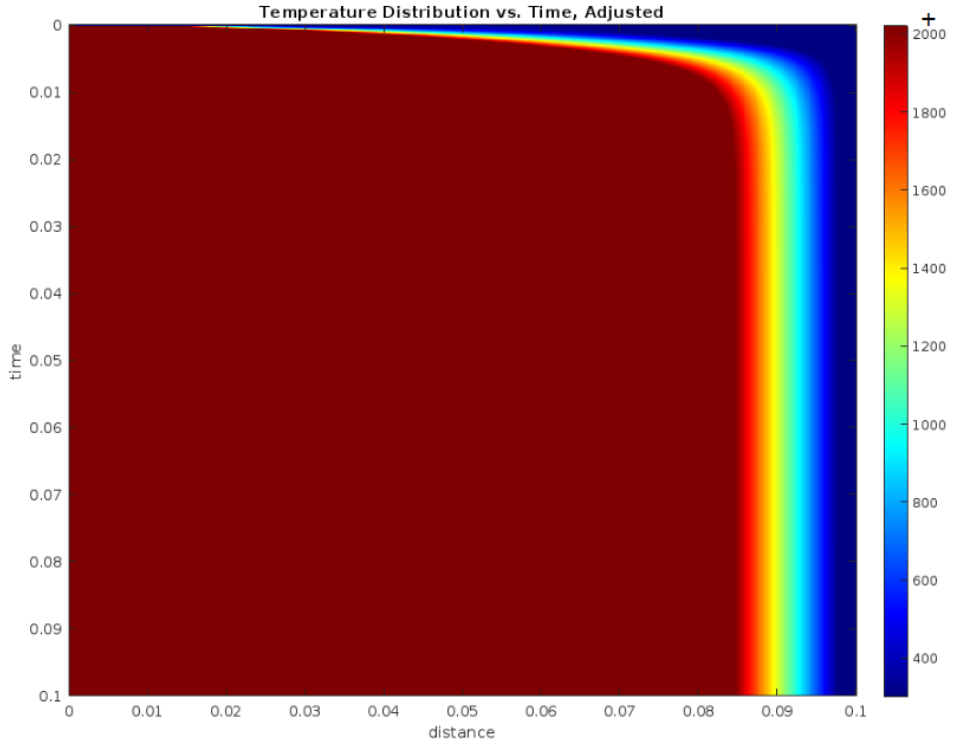

Figure 2.9: Adjusted temperature distribution versus time

From the graph, the damage falloff stops at approximately 0.03 seconds, representing the time where the heat diffusion starts to taper. It can be assumed that given an infinite amount of time, the depth of the vaporization will stay at a maximum of approximately 0.085 meters, given that no external factors are involved.

2.4 Heat Diffusion Model Discussion

2.4.1 Limitations on the Discretization of Space and Time Derivatives

As previously stated, the finite difference method uses the relation between the time derivative and space derivative to solve the thermal diffusion equation. When discretizing the time and space derivatives, more elements and finer element size result in more accurate results. However, increasing the number of elements leads to a greater consumption of computing power. MATLAB, the computational system of choice for this project, has a limit of 32.0 GB of computing power. A possible way of increasing accuracy while conserving computing power is

the implementation of varying mesh element sizes for the space derivative discretization. An example of a space discretization with varying element size is given in Figure 2.10:

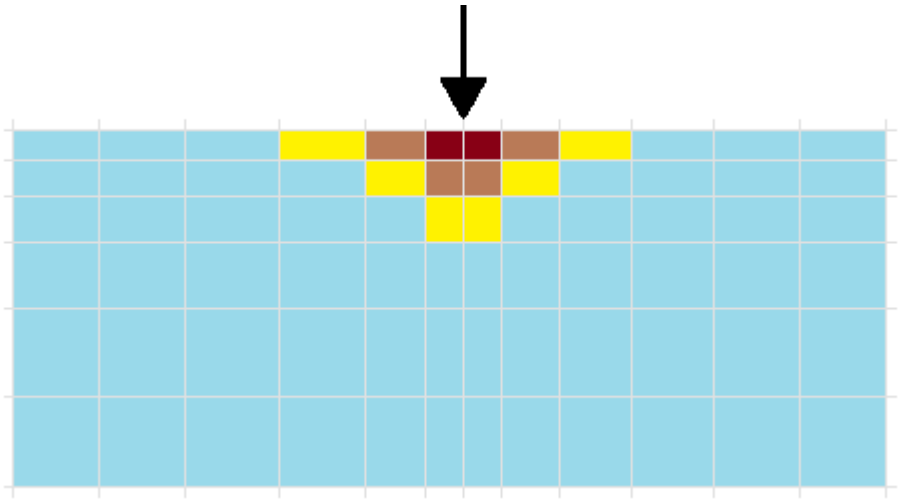

Figure 2.10: Varying element size space discretization

Although the grid sizing changes based on the input parameters, the element size could decrease in size closer to the impact point of the laser, increasing in size with an increase in distance away from the laser. This would allow the elements to have more accurate results where more damage is expected, while further elements that will be less affected by the laser have a coarser design. The MATLAB design for the base version of this model runs on an iterative system with equally sized grid elements. Due to the nested loop, changing the size of one element would change all other elements within its respective row or column (depending on the loop). Changing element size manually would require more work and is limited in possibilities by the nested loop setup in the code, but a simple version can be changed to have a constant increase in size proportional to the row or column number. The fineness of elements can be adjusted on a case-by-case basis while performing an error analysis to find the convergence of results.

2.4.2 Temperature Assumptions

Since the temperature distribution when comparing depth and radius in a Gaussian model follows an exponential curve, the temperature can never be fully accurately approximated in the initial conditions. Thus, the initial condition curve must be defined in a way that best represents the original temperature curve. Each grid element is defined by a constant value, meant to represent the temperature at any point within the coordinates of that area in the space derivative discretization. For this study, the constant temperatures defined for the grid elements were chosen using the largest initial condition, which used the largest temperature value within the space grid and applied it to the entire element.

A results analysis was performed to compare results using the largest temperature value to results using the temperature of the median point within the element. The initial conditions are given in Table 2.6:

Table 2.6: Initial conditions color map, largest vs. median approximations

Case	Red	Orange	Yellow	Green	Blue
Largest	1112 K	980 K	887 K	765 K	565 K
Median	1084 K	915 K	785 K	690 K	520 K

The heat diffusion behavior with respect to depth of the target surface is shown for both cases in Figure 2.11:

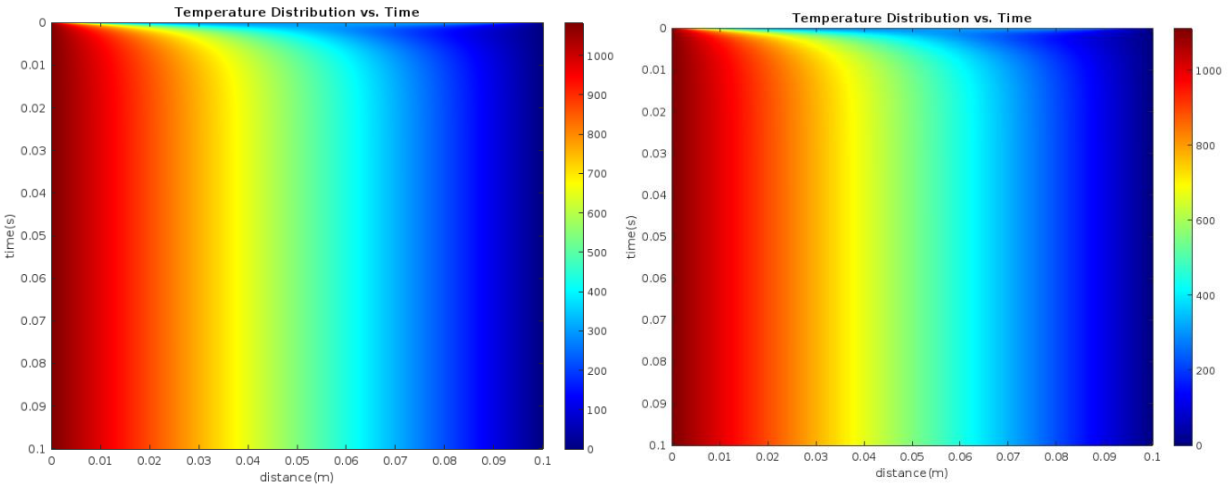

Figure 2.11: Heat diffusion behavior with median coordinate versus largest initial conditions

The behavior of the graph shows little difference in terms of curvature, as well as the estimated depth of damage curves. This may be due to the relative size of the laser and impacted elements with respect to the length of the target surface. The notable difference in the results is the maximum temperatures. Since the two cases use different initial conditions, the maximum temperatures in the distribution will be different depending on the maximum temperature found in the initial conditions. For the purpose of this study, the largest temperature in each grid is used as the initial condition to best represent the maximum temperature in the target surface during the heat diffusion process.

3. Finite Element Modelling

3.1 Initial Modeling

The purpose of this chapter is to develop a finite element model of laser impact in ANSYS. Compared to the previous models built in MATLAB, a finite element model allows for a three-dimensional representation of damage, more complex non-constant property values, and the possibility of estimating structural performance through other ANSYS modules.

Heat flux can be defined as the amount of thermal energy flowing through a specific area of the target surface. To obtain the heat flux of a laser, the energy density and pulse time can be used as follows [9]:

$$\phi = \frac{energy\ density}{pulse\ time} \tag{3.1}$$

where ϕ represents the heat flux. The energy density of the laser is obtained using the laser ablation simulation. The formula for energy density of a pulsed laser of circular shape is given as follows [9]:

$$energy\ density = \frac{pulse\ energy}{\pi(focal\ radius)^2} \tag{3.2}$$

As a baseline for creating a finite element model, the problem conditions from the MATLAB simulation were used. Using the calculated energy density from the laser ablation simulation, the heat flux can be derived for a given case. Thus, the laser properties used as an input for the laser ablation simulation can be converted into a heat flux value used as an input for the finite element model.

The geometry of the base model was modelled as a rectangular plate. The target surface face was designed as a square with a length of 10 millimeters, with a depth of 2 millimeters. From the results of the initial MATLAB test, which indicated melting damage in a very localized area for a plate with a side length of 200 millimeters, the scope of the finite element model was reduced to ignore areas of the plate far away from the impact location. The center of the rectangular plate contains a circular sketch zone, representing the location of the laser impact. The dimensions of the circular sketch can vary depending on the laser properties. For the initial case, the radius of the circle is 0.5 millimeters, matching the input for the laser ablation simulation. The geometry of the initial model is shown in Figure 3.1:

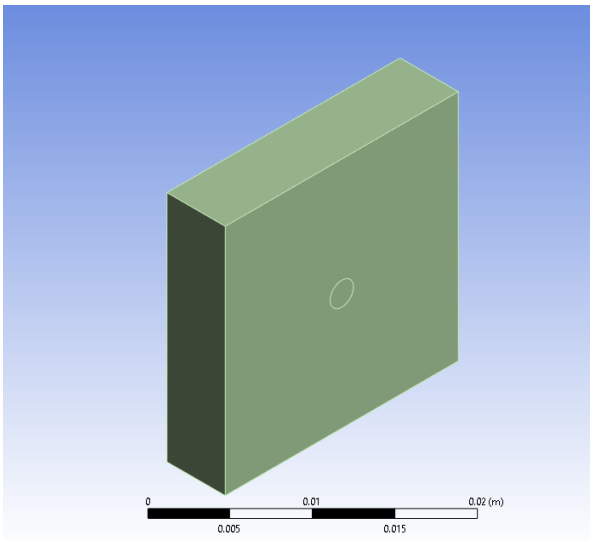

Figure 3.1: Finite element model geometry

The laser impact was modeled using a heat flux boundary condition in ANSYS Transient Thermal. The heat flux is applied to the circular zone on the target surface as shown in Figure 3.2, where the heat flux boundary condition is represented in blue:

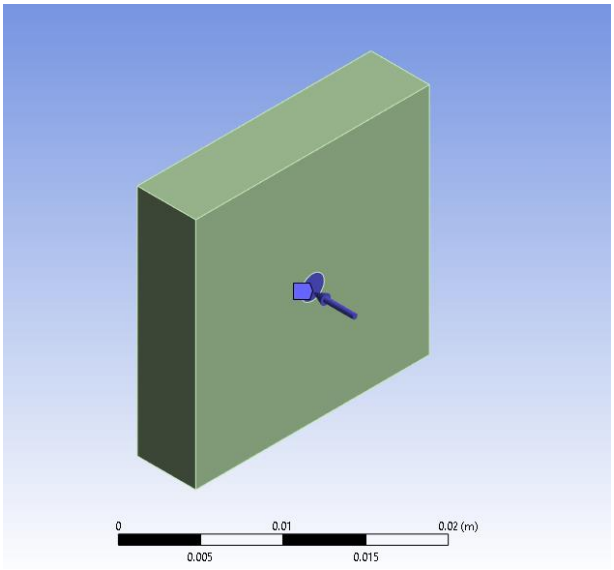

Figure 3.2: Boundary conditions

The remaining surfaces on the geometry, including the rest of the target surface face not impacted by the laser, are modeled with a convection boundary condition with the ambient temperature. For the initial model, this was set to 30 degrees Celsius, matching the test case in Chapter 2.
The mesh used in the initial model is relatively coarse, meant to improve processing time in order to verify that the model can run properly. Two separate mesh size conditions were set on the target face, with the heat flux zone having smaller elements than the remaining areas of the target face.

This is intended to improve the accuracy of results close to the laser impact, as that is the most critical area to study damage in. The initial mesh is shown in Figure 3.3:

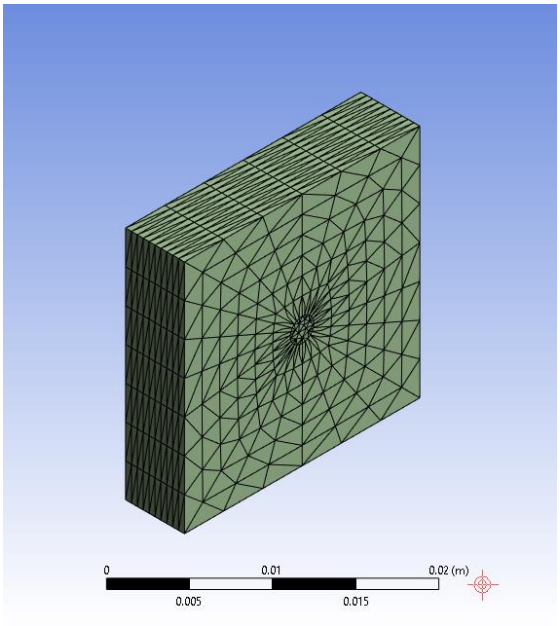

Figure 3.3: Initial mesh

The titanium material properties are given in Table 3.1. These values are relatively similar to the material property input of the MATLAB simulation, but contain variable tabular data, compared to the constant data in the MATLAB simulation.

Table 3.1: Titanium material properties

Common Material Properties	
Density	2700 kg/m³
Young's Modulus	table(T) = 7.0416e+10 Pa
Thermal Conductivity	table(T) = 236.31 W/m·°C
Specific Heat	table(T) = 894.35 J/kg·°C
Tensile Yield Strength	2.498e+07 Pa
Tensile Ultimate Strength	5.792e+07 Pa
Nonlinear Behavior	True
Full Details	Click To View Full Details

Note that there are material properties for structural performance included in the material properties. These values do not affect the temperature distribution from the laser impact but were included in the model for future calculations of structural damage with other ANSYS modules.

3.2 Initial Model Results and Model Refinement

The goal of the initial finite element model was to establish a baseline model that was able to fulfill a few conditions. First, the initial model should be able to model the laser impact using one of the thermal effects found in ANSYS Thermal, which was done using a heat flux boundary condition. Second, the initial model does not need to provide accurate results but should have results that can be improved upon in future iterations of the model. The heat flux temperature distribution results and corresponding legend are shown in Figure 3.4:

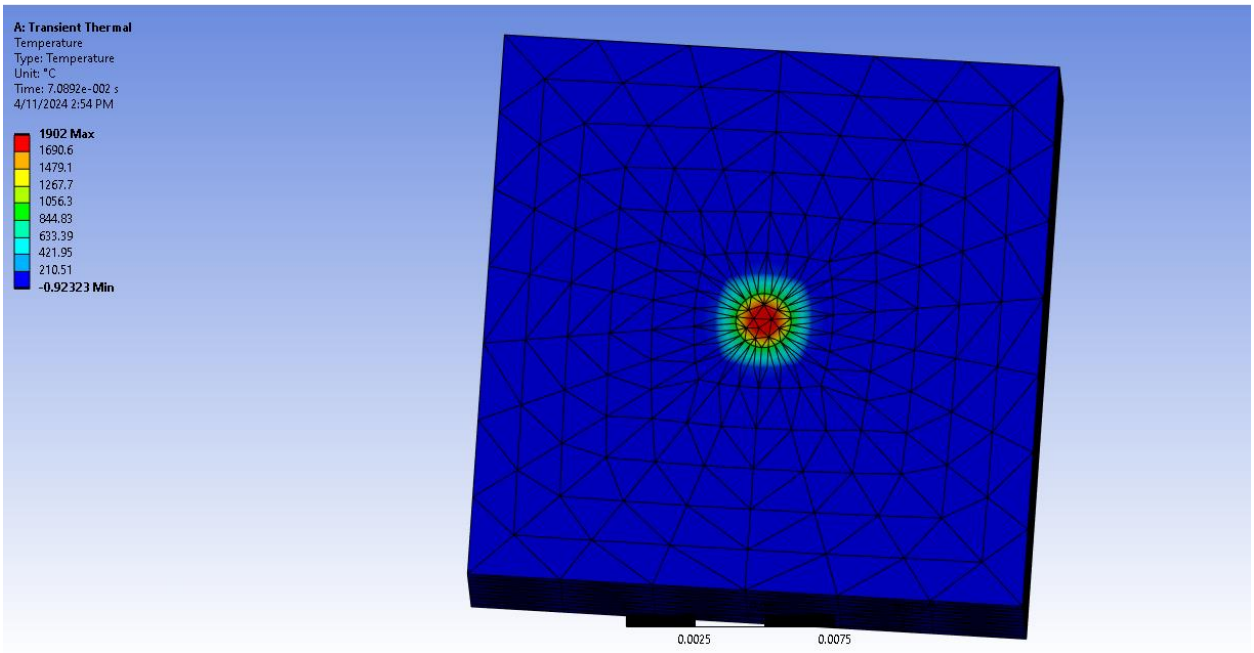

Figure 3.4: Temperature distribution

The maximum temperature of the finite element model is 1902 degrees Celsius, whereas the maximum temperature of the MATLAB model is 3032 degrees Celsius. Most of the temperature distribution is located in the area within 1 millimeter of the original laser impact. In terms of positives, the initial model resulted in temperatures indicating damage along the target surface. The vaporization temperature of titanium is approximately 1750 degrees Celsius, which indicates that a localized section about the center of the heat flux boundary condition undergoes enough of a temperature increase to cause damage from vaporization during the laser impact. However, the damage is extremely localized, which results in a smaller radius of damage than expected from the MATLAB model. Most of the temperature increase is in the area within the heat flux boundary condition, resulting in a damage radius smaller than the applied laser's.

Some of the discrepancies between the MATLAB and finite element simulations may be due to the non-constant material properties in the finite element model. The MATLAB model is

more of an approximation due to the constant material properties, but these material properties change at certain temperatures as represented in the finite element material properties.

Another reason for a discrepancy in maximum temperature results can be attributed to the element choice and sizing of the mesh. In the initial model, the mesh was relatively generic, with the goal of reducing calculation time. The sharp elements located next to the impact zone may have led to less accurate calculations. This version of the finite element model took approximately 2 minutes to perform. A future step to developing the finite element model is to create a more detailed mesh using concentric rings of elements, as well as decreasing the element size. From the preliminary results of this initial model, it appears that the most important location in the model is the area located on and directly next to the laser impact location. Thus, a smaller element size would be used in this area, with increasing element size further away from the impact to save calculation time. From a new mesh design, a mesh refinement study can be performed with a test case, reducing the element size until temperature distribution results converge.

3.3 Model Improvements

3.3.1 Time-Step Changes

In the initial model, the heat flux of the laser was calculated using Eq. 3.2, which states that the total heat flux absorbed by the target surface is equal to the energy density of the laser divided by the exposure time. Note that the heat flux is used interchangeably with energy density in the case of this model. In the initial model, the global minimum time step was set to 10^-4 seconds, the default value defined by ANSYS. This caused an error with accurately modelling the laser impact in ANSYS, as the exposure time from the MATLAB case was 100 nanoseconds. To more accurately compare results from the finite element model to the MATLAB model, the global time step must be changed to accommodate time values within the laser's exposure time.

	Steps	Time [s]	Heat Flux [W/m²]
1	1	0.	= 6.366e+010
2	1	1.e-007	6.366e+010
*			

Figure 3.5: ANSYS time step data input for initial model

To avoid the time step issue in the initial model, the initial model scaled the energy density of the laser so that the equivalent absorbed heat flux would be the same regardless of the exposure time. For the second iteration of the model, where the time step issue was identified and fixed, the energy density was set to the same energy density found using the laser ablation simulation [9]. Using Eq. 3.2, a comparison of the heat flux input and exposure time for each model are shown in Table 3.2:

Table 3.2: Heat flux time modelling comparison

Case	Energy Density($\frac{W}{m^2}$)	Exposure Time(s)	Energy/square meter($\frac{J}{m^2}$)
Initial	6.366×10^{10}	10^{-7}	6.366×10^{3}
Second	6.366×10^{7}	10^{-4}	6.366×10^{3}

One of the issues with inaccurate time step modelling was the exponential growth of error throughout multiple time steps during the analysis process. Any error found in a step propagates to the following time step, which continues to affect every following time step after it. Thus, although the total heat flux absorbed throughout the analysis process would be the same across the two models with varying analysis time, the error in between time steps could result in a significant change in analysis results. In addition, using too large of a time step can result in an inaccurate estimation of results, such as approximating the area underneath a curve using rectangles. The energy density input was defined as a constant from the initial time to the final time, but the analysis process had multiple steps between the initial and final time. To mitigate the estimation error by using too few time steps, the number of time steps was increased in the second iteration. In order to do this, the global minimum time step had to be decreased enough to allow for an increase in time steps. To accommodate an increase from 10 time steps to 100, the global minimum time step was set to 1 nanosecond. Thus, the time-step modifications for the second iteration resulted in a model with 100 time steps with a duration of 1 nanosecond, resulting in a total exposure time of 100 nanoseconds. For reference, the first five entries and last five entries of the time steps are shown in Figure 3.6:

	Time [s]	Minimum [°C]	Maximum [°C]	Average [°C]
1	1.e-009	31.025	319.16	109.54
2	2.e-009	-15.801	320.93	103.65
3	3.e-009	-58.588	346.9	104.91
4	4.e-009	-101.84	370.44	105.4
5	5.e-009	-145.1	394.46	105.98
96	9.6e-008	-4061.1	3092.9	155.21
97	9.7e-008	-4090.1	3117.1	155.79
98	9.8e-008	-4118.8	3141.4	156.39
99	9.9e-008	-4147.4	3165.7	156.98
100	1.e-007	-4175.8	3189.9	157.58

Figure 3.6: ANSYS time step data input for second model

3.3.2 Geometry and Mesh Changes

The initial model was built using a rectangular prism of length and width of 10 millimeters and a depth of 2 millimeters. From the temperature distribution results in Figure 3.4, it can

reasonably be assumed that the main area of focus is the elements within the heat flux boundary condition and the localized area around the impact. In the model's second iteration, the geometry of the rectangular prism was reduced to save computational time and allocate more elements in the localized area of study.

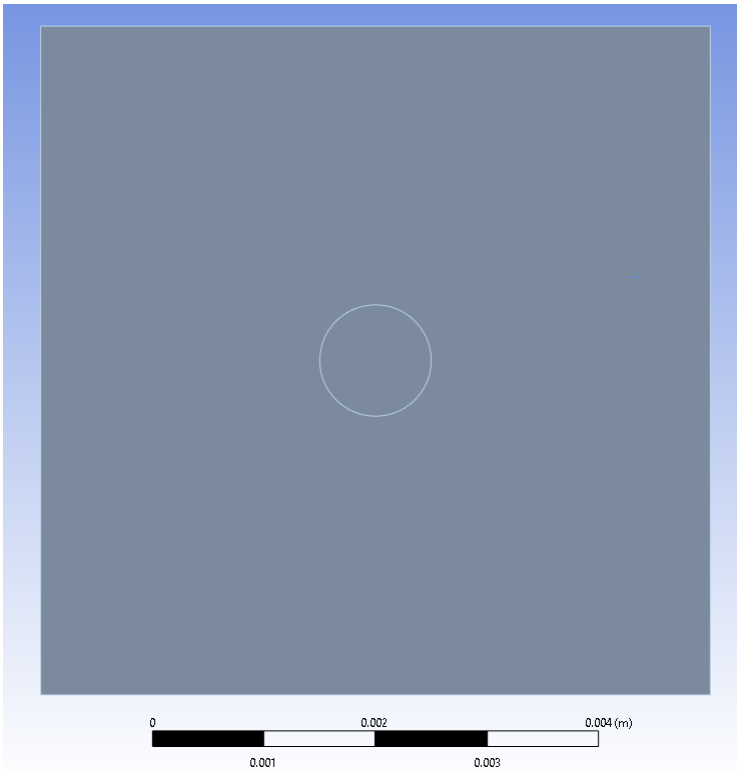

Figure 3.7: Second model geometry with reduced size dimensions

In addition to a change in total geometry, the mesh elements were redefined to have smaller dimensions due to the reduction in computational time afforded by the reduction in geometry. These values were assigned relatively arbitrarily, as the purpose was simply to test results and computational time for a smaller mesh element size relative to the initial model. The dimension comparison between the two cases can be found in Table 3.3:

Table 3.3: Comparison of computational time for different geometry and inner element size

Case	Inner Element Size(m)	Dimensions(mm)	Computational Time(s)
Initial	5×10^{-4}	$10 \times 10 \times 1$	0.03
Second	5×10^{-5}	$6 \times 6 \times 1$	0.05

Another possible reason for a variation in results can be attributed to the shape of elements used in the meshing process, as sharp boundaries at nodes where many elements meet can result

in relatively extreme values. These sharp elements can be seen in the initial model, as shown in Figure 3.8:

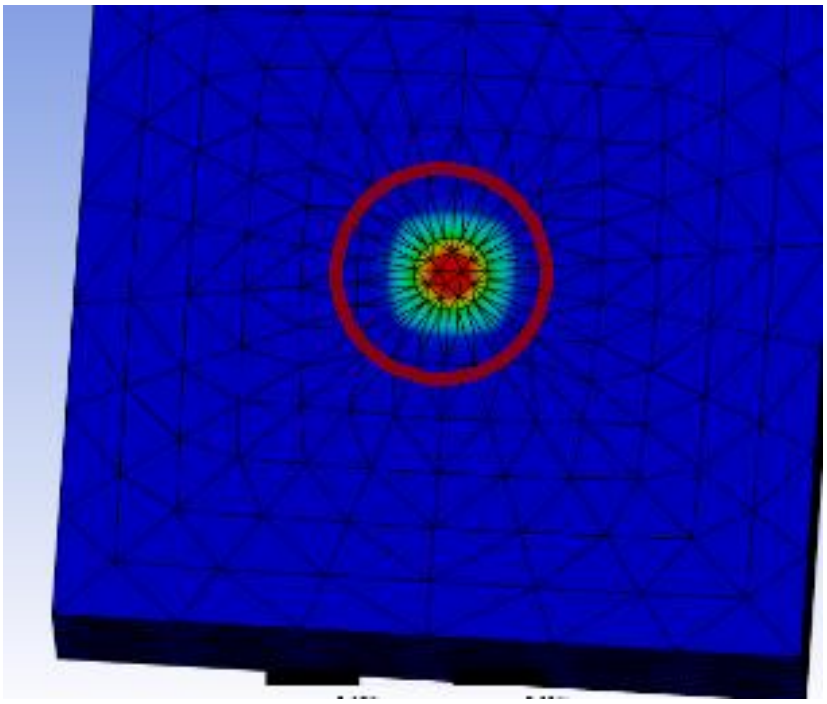

Figure 3.8: Critical sharp elements in initial mesh

To refine the model, it was necessary to redefine the meshing conditions of the model to avoid these kinds of elements. In the initial model, meshing was performed using a zone-defined element size, where an element size was defined for a user-defined region in the geometry and automatically meshed to fit that condition. This meshing was performed in two different mesh condition zones: the outer zone located outside of the laser impact, and the inner zone located within the area of contact with the laser.

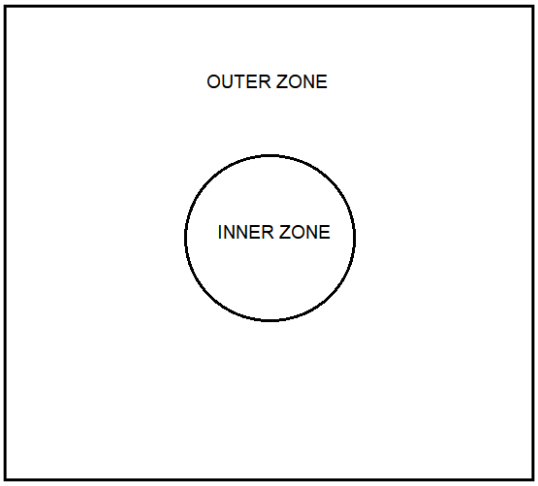

Figure 3.9: Inner and outer meshing zones

While this method was effective by making the element size simple to tune, it resulted in unwanted sharp element shapes. In the second model, the mesh was defined using a concentric circle method, in which a series of concentric rings of mesh elements about the circular shape of the laser impact would be defined using nodes. The number of nodes was kept the same through an increase in radius, as the elements further away from the laser impact were deemed as less necessary to study as shown from the temperature distribution results of the initial model study. An example of a node-defined mesh is shown in Figure 3.10:

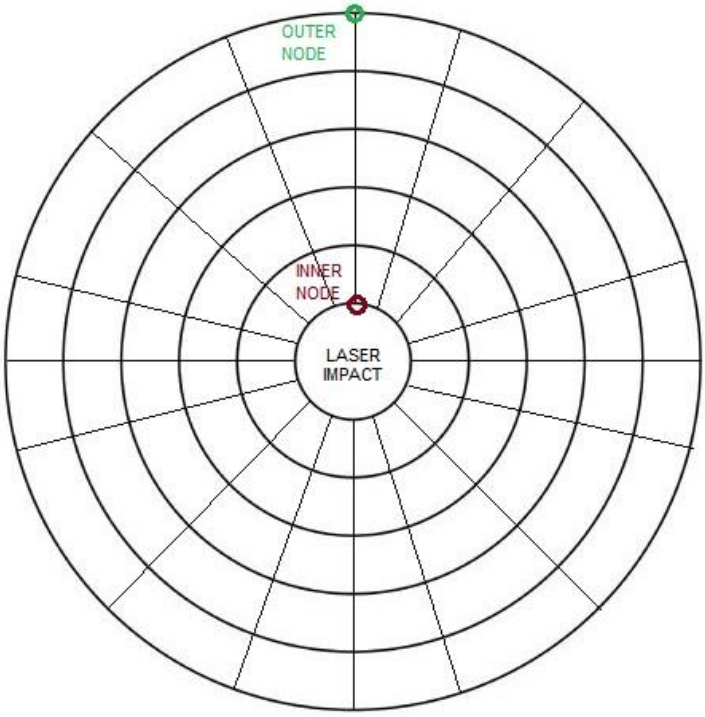

Figure 3.10: Example of node-defined concentric mesh

This was performed in ANSYS using an edge sizing condition. For the second study, the mesh rule was set to 25 nodes. Note that since the mesh rule must have the same number of nodes on the outer ring as the inner ring, the concentric design will taper off for elements further away from the inner surface. However, since the area in question is the area surrounding the inner edge, this should not affect the maximum temperature results. The edge sizing condition used in ANSYS is shown in Figure 3.11.

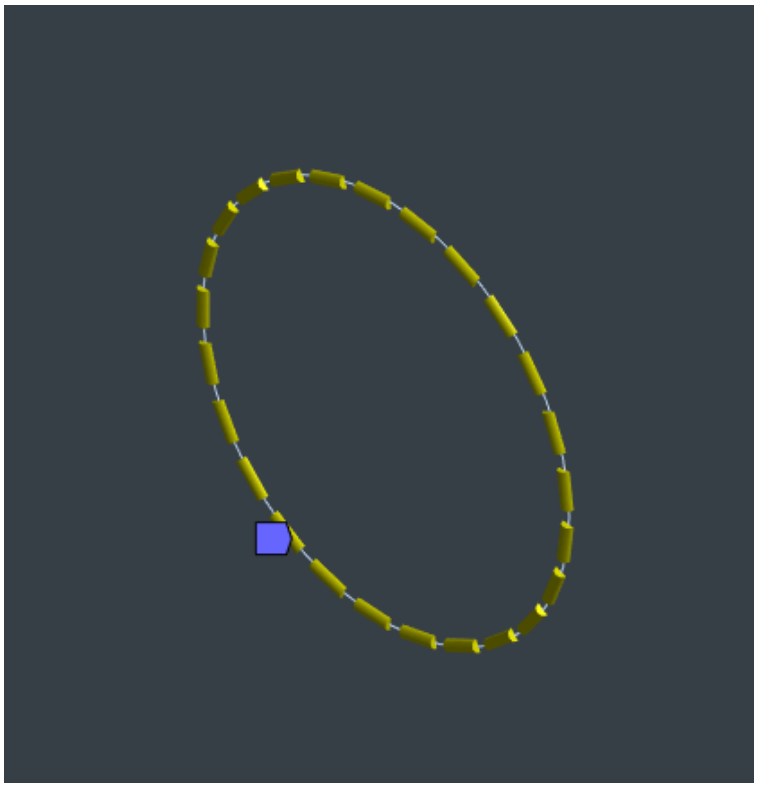

Figure 3.11: Edge sizing condition with 25 nodes

The concentric circle meshing condition was only defined for the outer zone because the element size would drastically decrease closer to the center of the inner zone. The node meshing condition in ANSYS is defined using the same number of nodes from an inner and outer surface, which are shown in Figure 3.11. To have a concentric node meshing condition in the inner meshing zone, a center point would need to be defined at the center of the inner zone, which would then have 25 nodes applied. This would result in extremely sharp elements in the middle of the inner zone, potentially resulting in errors in the most critical part of the model. To mitigate the sharp elements found in the inner zone, the inner zone was meshed using an element size mesh condition using triangular elements. The disadvantage of using triangular elements is that the temperature distribution will not be perfectly symmetrical about the center of the laser impact due to asymmetry in the mesh, but the results should be close enough that the slight variation of temperature distribution can be ignored. As the mesh element size is gradually reduced through a mesh refinement study, this asymmetry will become less prevalent.

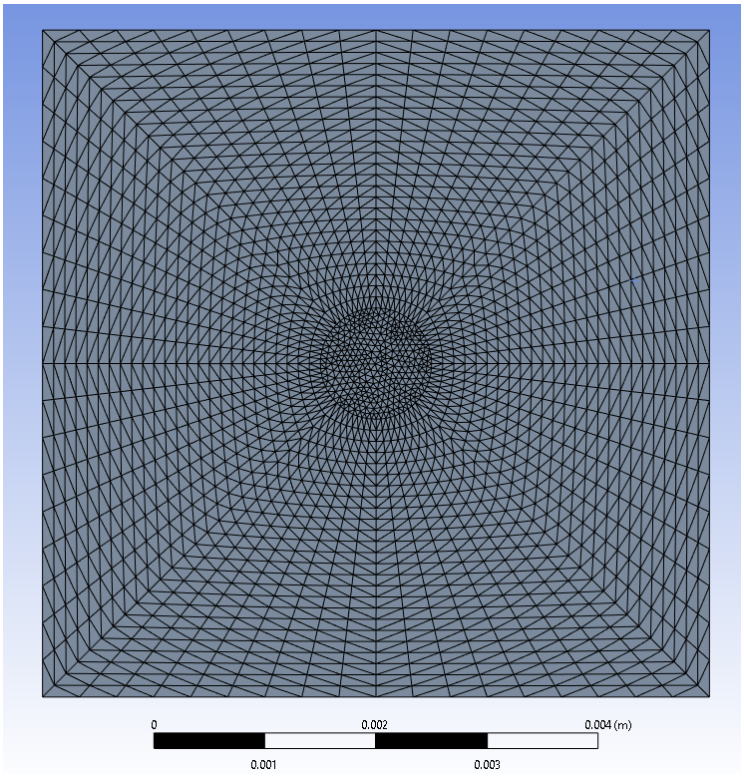

Figure 3.12: Initial mesh for the second model

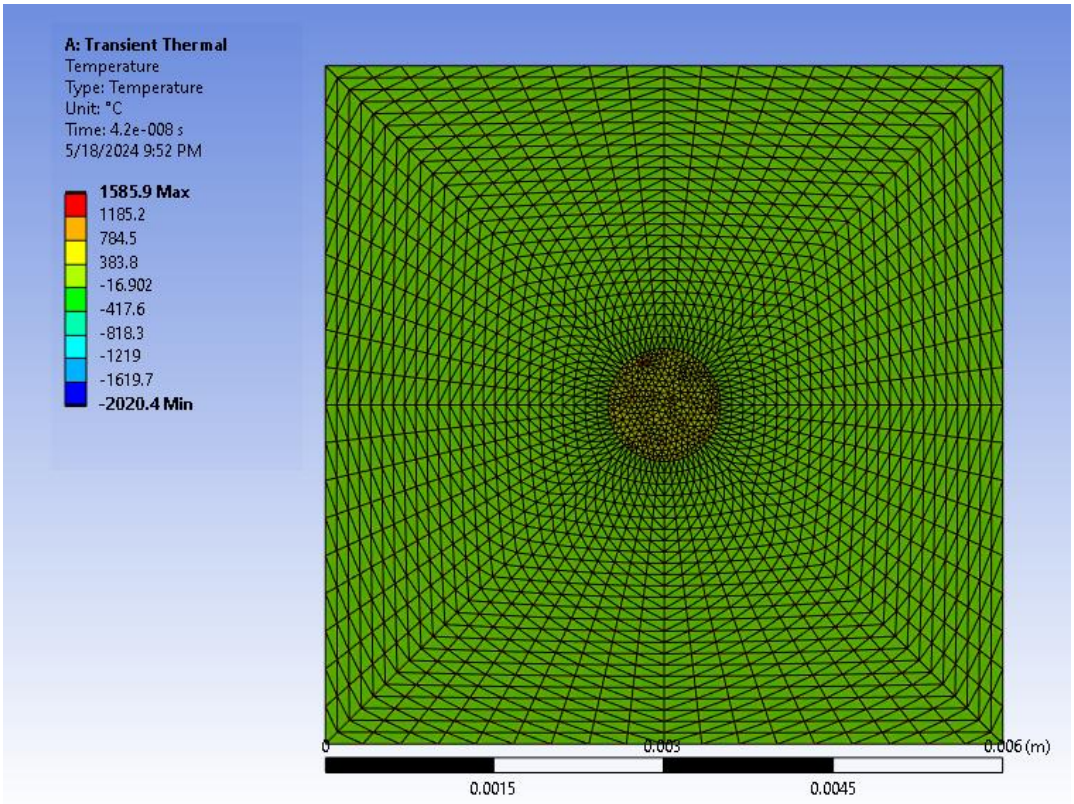

Figure 3.13: Initial meshing temperature distribution

To find out if the temperature distribution results will converge, a mesh refinement study was performed. This allowed the mesh element size, maximum temperature, and computational time to be compared. Once results were established for cases with varying element sizes, a final element size can be chosen to optimize the three factors previously stated. In each step of the mesh refinement study, the element size was reduced to one half of the element size in the previous step. This was to be repeated until the maximum temperature converged to a tolerance of 5 percent or until the computational power exceeded that of the computer used for the study. The mesh refinement study results can be found in Table 3.4:

Table 3.4: Mesh refinement data

Element Size(m)	Maximum Temperature(C)	Computational Time
$\mathbf{5 \times 10^{-5}}$	1585.9	0:05
$\mathbf{2.5 \times 10^{-5}}$	5742.8	0:49
$\mathbf{1.25 \times 10^{-5}}$	4576.3	2:47
$\mathbf{6.25 \times 10^{-6}}$	2872.4	12:39
$\mathbf{3.125 \times 10^{-6}}$	N/A	N/A(20:00+)

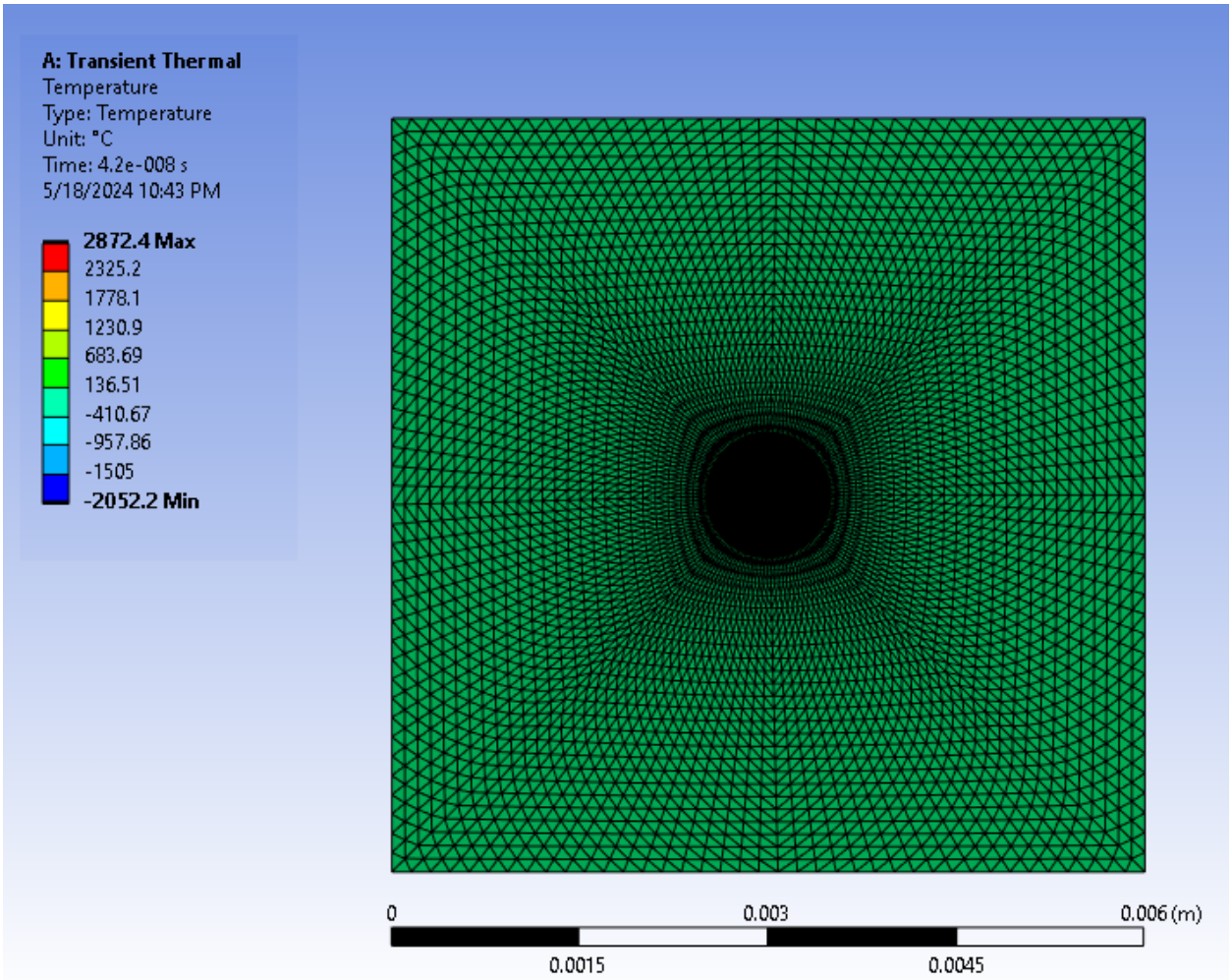

Figure 3.14: Temperature distribution after mesh refinement

A version of the temperature distribution with focus on the inner meshing zone is shown in Figure 3.15:

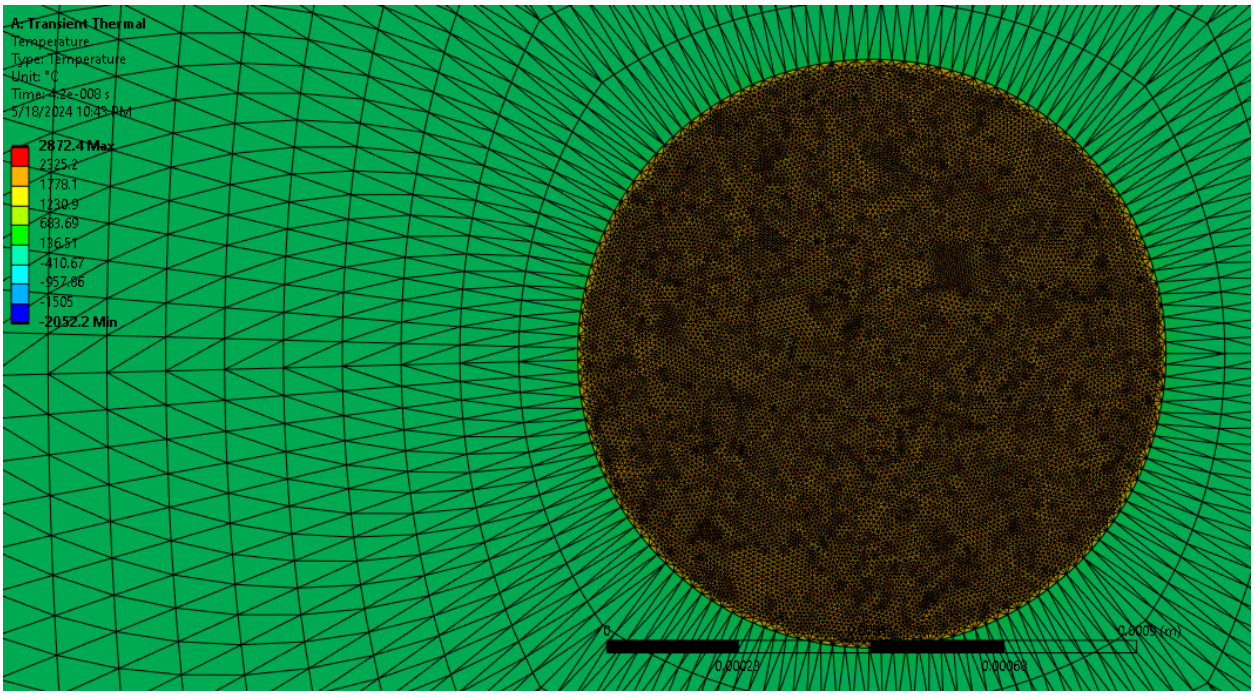

Figure 3.15: Laser impact localized temperature distribution

The change of the maximum and average temperature over time is shown in Figure 3.16, where the maximum temperature is in green, and the average temperature is in blue:

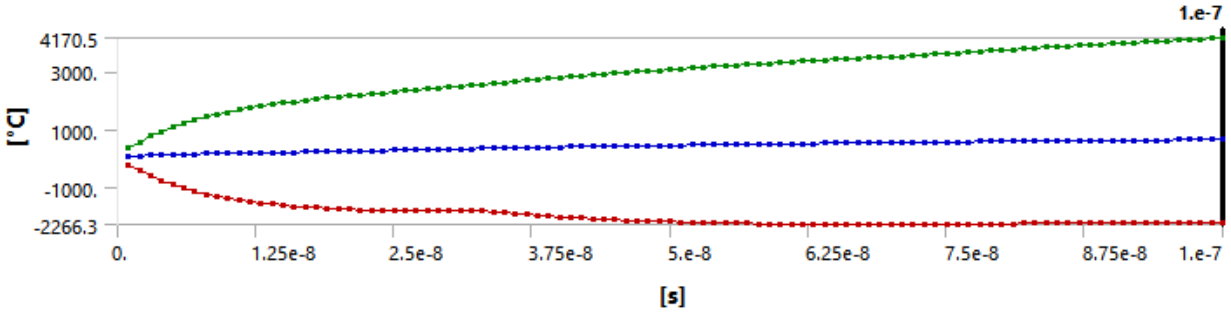

Figure 3.16: Temperature distribution over time

Note that the mesh refinement study was only performed for mesh elements in the inner meshing zone. In the first iteration of the mesh refinement study, as well as in the results from the initial model, it was observed that the maximum temperature occurs within the inner meshing zone. In addition, the heat flux was only applied to the geometry associated with the inner meshing zone, where the assumption was made that the maximum temperature will never be located outside of the inner meshing zone for a case with a singular laser impact. Thus, the decision was made to only refine the mesh of the inner meshing zone to save time and avoid increasing the number of elements where it was deemed less necessary.

Due to a computational power issue with the computer used for this study, the element size could not be decreased past a size of 6.25×10^{-6} m. When an element size of 3.125×10^{-6}m

was used, the ANSYS analysis resulted in the computer crashing and an incomplete result file. This error occurred approximately 20 minutes into the analysis over two tries. Thus, the decision to stop the refinement at an element size of 6.25×10^{-6} was chosen. The maximum temperature at this step of the mesh refinement study.

3.4 Model Comparison and Future Steps

The error percentage of the results with respect to the MATLAB results can be calculated using the following equation:

$$error\ \% = \left|\frac{estimated-actual}{actual}\right| \times 100 \tag{3.3}$$

where the value from the MATLAB laser simulation is represented by the actual value, whereas the temperature value from the finite element simulation. A comparison of the initial model and the second model with mesh refinement is shown in Table 3.5:

Table 3.5: Initial versus second model comparison

Inner Element Size(m)	Maximum Temperature(C)	Computational Time	Error %
$\mathbf{5 \times 10^{-4}}$	1585.9	0:03	47.69%
$\mathbf{6.25 \times 10^{-6}}$	2872.4	12:39	5.26%

Compared to the initial finite element model, the difference between the maximum temperature results of the second finite element model and the results of the MATLAB model are significantly smaller. The second model results in a maximum temperature of 2872.4 degrees Celsius, while the MATLAB study results in a maximum temperature of 3032 degrees Celsius. The second model reduces the total size of the geometry, allowing the analysis to closely study the area around the laser impact in which the maximum temperature is expected to occur. In addition, the second model uses more time steps, which reduces the error that results from using inadequately large time steps for approximation. The second model also fixed the global minimum time step issue that arose in the first model. Finally, the mesh was refined to have smaller elements and use a concentric mesh pattern to avoid error resulting from sharp finite elements.

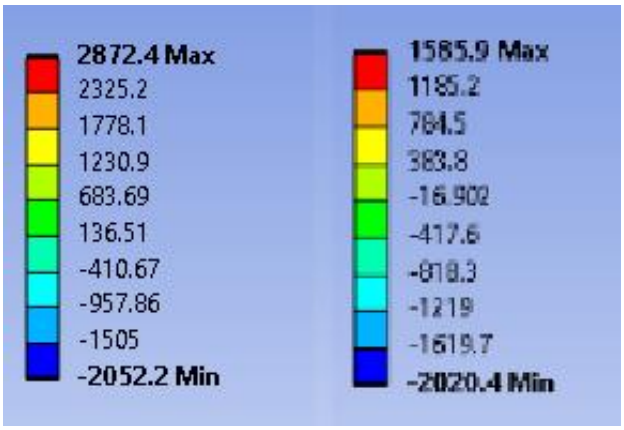

Figure 3.17: Temperature differences between refined and initial model

To further improve on the changes made in the second model, the geometry can possibly be further reduced into a more extreme version that only includes the inner meshing zone and the immediate surrounding elements. This would result in geometry being a cylinder with a radius of slightly greater than 1 millimeter and depth of 1 millimeter. Although this would greatly reduce the computational power and time by removing a significant number of elements, it prevents the addition of a convection study during damage analysis. As previously observed in the MATLAB study, the laser impact results in a maximum temperature greater than the vaporization temperature of the material. However, in the time immediately after the laser exposure, the temperature will propagate radially about the laser impact in the cross-section of the target surface. Thus, having elements in the area surrounding the laser impact is important to understanding the convection behavior of the target surface in the time after the laser impact, as some areas may undergo damage from melting after the laser impact, increasing the radius of damage. To further refine a third model, a convection damage study must be performed in order to understand which elements can be considered not at-risk of damage similar to the MATLAB study in Chapter 2.

In addition, the current model studies the maximum damage radius, which occurs directly on the impacted surface. A future improvement to the model must include a method to depict three-dimensional damage throughout the depth of the target surface, which should behave like the Gaussian damage profile shown in [10]. One possible way to model this is to visually remove all damaged elements from the view of the model after the final time step, which would provide an estimation for the physical appearance of the target surface after impact. This damage assumption is made assuming that all elements with a temperature greater than the vaporization temperature of the material would ablate away, thus allowing it to be visually removed from the model.

Finally, this finite element model was modelled using titanium, which is an isotropic, uniform material in this case. To properly study damage from a laser impact to a composite structure, the target surface must be redesigned using a composite laminate, where laminate properties can be obtained within ANSYS. This allows for composite-specific damage, such as delamination and damage to the epoxy layer, to be quantified within the model, since the current iteration of the model uses a uniform material.

4. Model Verification

4.1 Test Case, T800/M21

4.1.1 Previous Study Results and Discussion

Ecault et al. perform a study on composite material damage due to laser shock waves, quantifying damage to composite structures experimentally [7]. Using a T800/M21 carbon fiber test specimen with a thickness of 6 millimeters, Ecault et al. characterized two methods of damage to the test specimen by laser impact. The material used in the study by Ecault et al. was T800/M21, a type of carbon fiber. The material properties for T800/M21 are shown in Table 4.1.

Table 4.1: T800/M21 Material Properties

UD tensile strength (MPa)	UD tensile modulus (GPa)	UD compressive strength (MPa)	UD compressive modulus (GPa)	45° in-plane shear strength (MPa)	45° in-plane shear modulus (GPa)	CAI at 6.7J impact (MPa)
2451	171	1231	148	145	5.1	280

1. Source: Hexcel data sheet.

One of the methods was analyzing blisters that occurred on the back face of the composite specimen, or the side that did not receive direct contact with the laser. Figure 4.1 depicts an example of the shape and dimensions of the back face deformation.

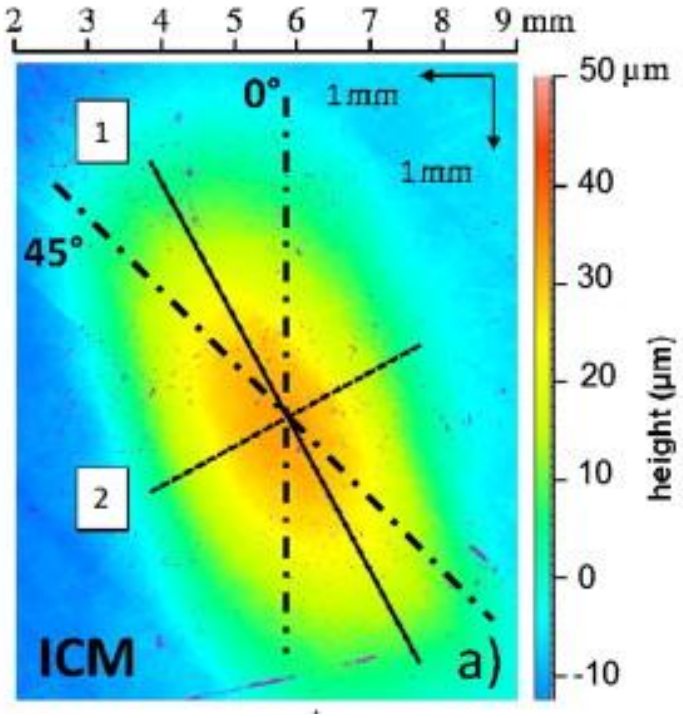

Figure 4.1: Experimental results for back face deformation [7]

Figure 4.1 shows an elliptical deformation pattern on the back face of the composite target surface. The maximum back face deformation for this case is approximately 40 micrometers, located in the area on the back face below the laser impact. The damage from the laser shock propagates in a cone-shaped pattern throughout the target surface [7]. As the deformation is small to the naked eye, Ecault et al. used X-ray radiography to observe the change in topography from the laser impact. It is noted that the loading from the laser impact is centered on a small spot of the target surface due to the high power of the laser. This behavior, combined with the cone-shaped propagation of the heat flux throughout the thickness of the target, results in a relatively focused back face deformation. In terms of modelling the laser impact with finite element software, this could potentially allow the dimensions of the target surface face to be reduced, as significant damage does not seem to occur away from the initial impacted area. This behavior matches up with the finite element modelling process in Chapter 3, where any elements that had temperatures exceeding the vaporization temperature of the carbon fiber were concentrated within the laser impact zone and the immediate surrounding elements. With the thickness of deformation being more important in this study, it allows the thickness of the model to be increased while conserving enough elements to remain within the computational limits of ANSYS.

The other criterion for damage presented by Ecault et al. is the maximum depth in which delamination occurs within the composite. Damage from delamination is not as visually prominent as the removal of material and change in geometry from vaporization, but still affects the stiffness

performance and structural integrity of the composite structure [7]. The relation between the delamination depth and the intensity of the laser are shown in Figure 4.2.

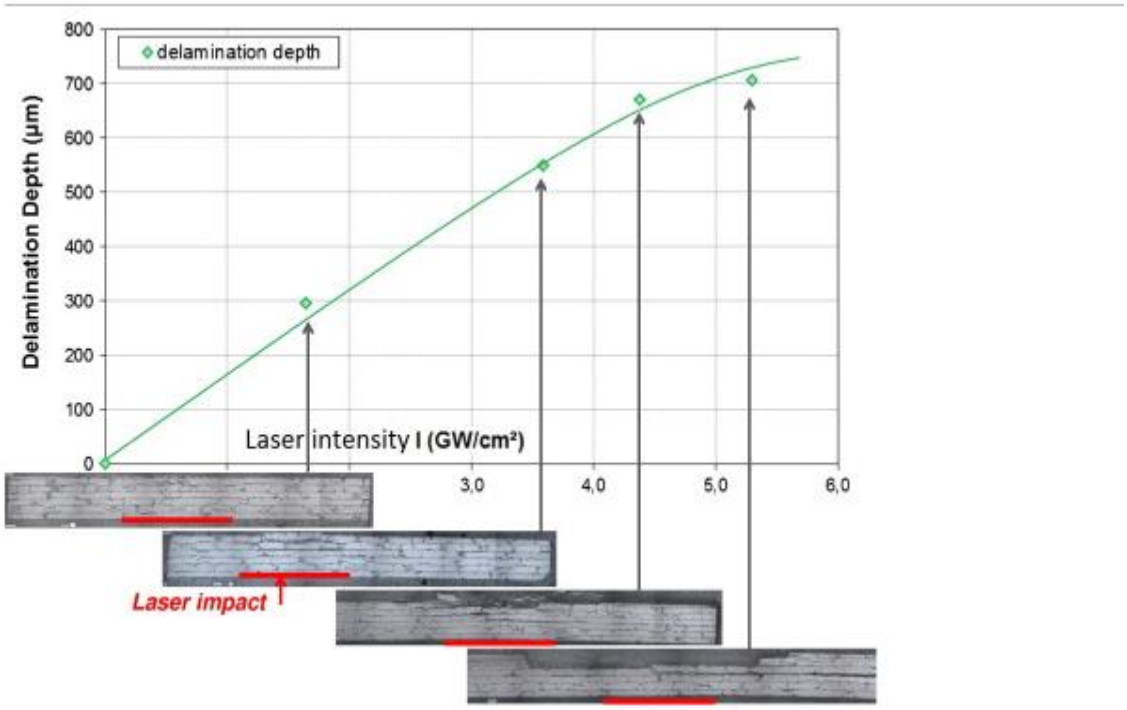

Figure 4.2: Experimental results for delamination depth [7]

Delamination damage commonly occurs when the matrix material of the composite structure is damaged. In carbon fiber applications, epoxy is used as the matrix material of the composite structure. To assume damage to the epoxy from heating, the glass transition temperature of the epoxy is used as a damage criterion. When the temperature of the epoxy layer exceeds the glass transition temperature, the material transitions from a hard and brittle state to a soft and pliable state [20]. As the integrity of the matrix material is compromised at a high temperature, the carbon fiber plies in contact with the compromised matrix would be at risk of delamination. In T800/M21, the matrix material is the M21 epoxy, which has a glass transition temperature of 185 degrees Celsius [20].

4.1.2 Finite Element Model Setup

To test the validity of the heat flux model, previous experiment setups should be recreated faithfully with the heat flux model to obtain a similar result. Comparing to previous study results as a benchmark allows the physical assumptions within the finite element model, as well as the model methodology, to be validated. In the case that the result from the experimental setup differs from the finite element model, adjustments can be made, refining the model until the results for

both the model and experiment produce similar results. Thus, the goal of the finite element model is to obtain similar behavior to one of the damage criteria described by Ecault et al. Judging from the nature of the previous test, in which vaporization damage was only found near the surface layer, it can be predicted that most of the deformation will occur within the extremely localized area of the laser impact.

The initial step in recreating the experimental setup is to determine which values and dimensions from the initial finite element model need to be changed. For example, the diameter of the laser impact developed in the initial model was 2 millimeters, whereas the diameter of the laser impact in the experiment was 4 millimeters. The depth of the composite plate in the initial model was 2 millimeters, whereas the depth of the composite plate in the experimental model was 6 millimeters. In the initial finite element model, where the laser diameter was only 2 millimeters, no damage was found within the bottom half of the 2-millimeter depth. However, an increase in the laser diameter with a 4-millimeter diameter would result in a greater heat flux. To match the back face deformation method of quantifying damage used in the experimental setup, the thickness of the composite sample in the new model was set to 6 millimeters.

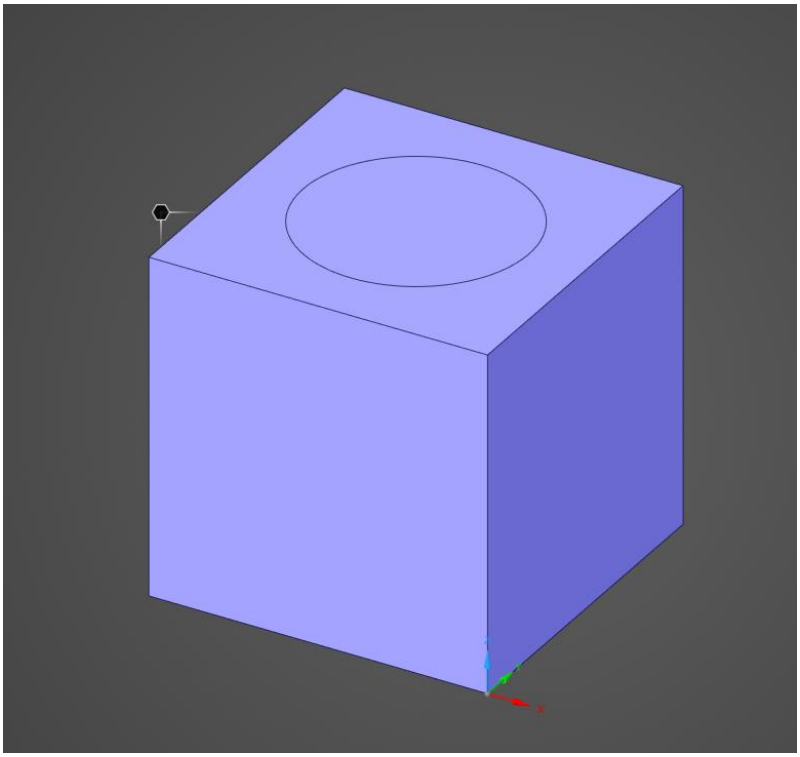

Figure 4.3: Geometry with modified radius and thickness

The material was changed to have the specific properties of T800/M21 carbon fiber. This material was not available in ANSYS, so a user-defined material was created to simulate T800/M21.

The finite element model was performed for a laser impact with characteristics described by Ecault et al. The laser shock properties used in the experimental setup are listed in Table 4.2:

Table 4.2: Laser shock wave properties [7]

Intensity	Focal Radius	Pulse Time
3.43 $\boldsymbol{GW/cm^2}$	2 mm	30 ns

The energy of the laser can be extrapolated from the conductivity, focal radius, and pulse time given in Table 4.2.

$$pulse\ energy\ =\ \frac{intensity*\pi(focal\ radius)^2}{pulse\ time} \tag{4.1}$$

The intensity of the laser can be directly used as the heat flux input within ANSYS, as both have units of power relative to area.

As an initial method to run the laser impact analysis, the initial mesh of the recreated experimental setup used the same meshing controls as the old model in Figure 3.12. However, due to the change in geometry of the laser impact zone, each of the mesh elements in the zone outside of the laser impact are larger than the previous iteration of the model. The complete view of the mesh is shown in Figure 4.4, while a subsection of the laser impact zone mesh is shown in Figure 4.5 for clarification.

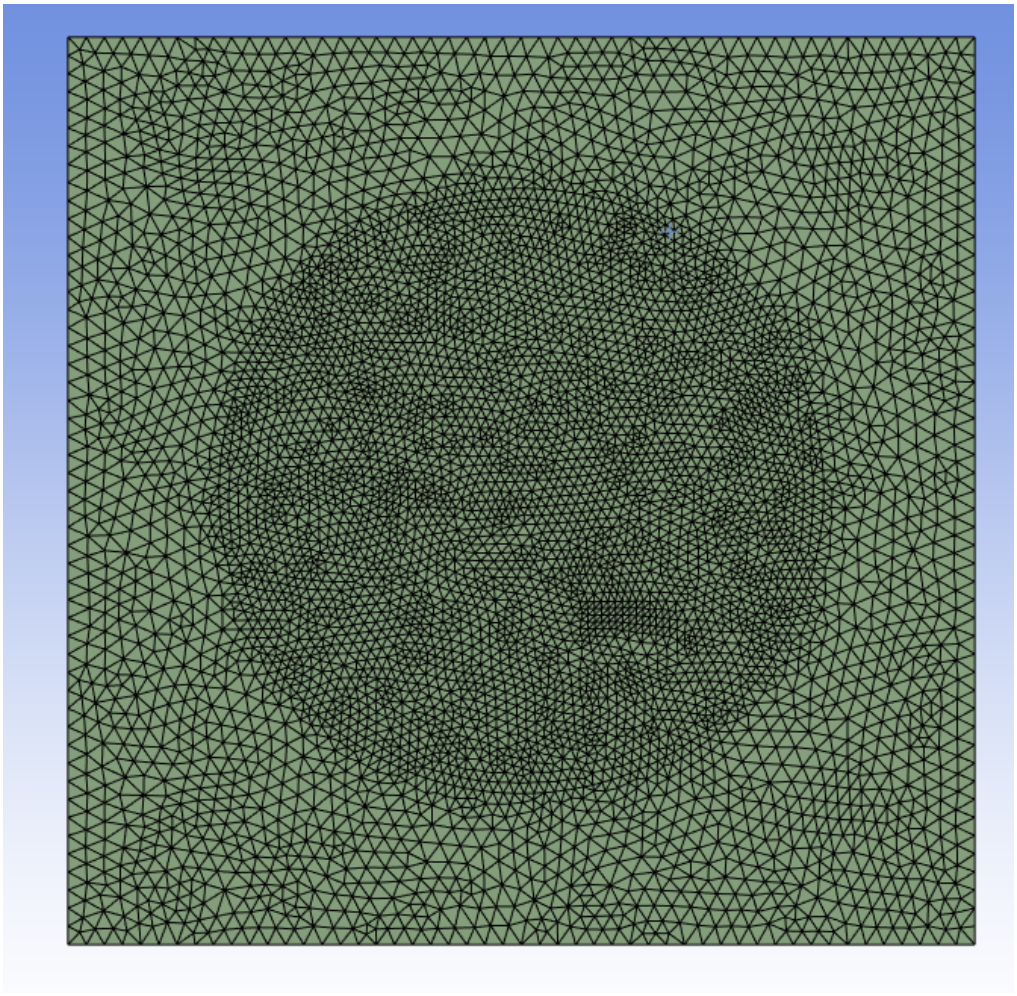

Figure 4.4: Mesh used for the experimental recreation

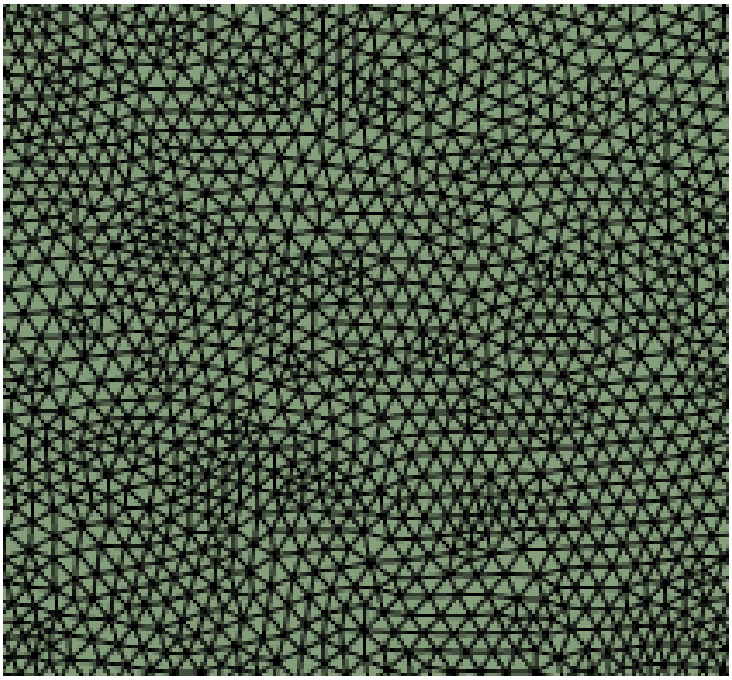

Figure 4.5: Close-up view of the laser impact zone mesh

4.1.3 Finite Element Model Results

Following the finite element model from Chapter 3, the deformation due to vaporization was obtained by the model. Elements where the temperature of the composite material exceeded the temperature of vaporization were assumed to be vaporized. Visually, these elements were removed from the finite element model, leaving a geometric representation of the deformed target after exposure. While the vaporization deformation is not a direct damage criterion described by Ecault et al., it is a useful supplement to understanding the coupled damage with the delamination depth. The deformed geometry of the T800/M21 structure due to vaporization is shown in Figure 4.6:

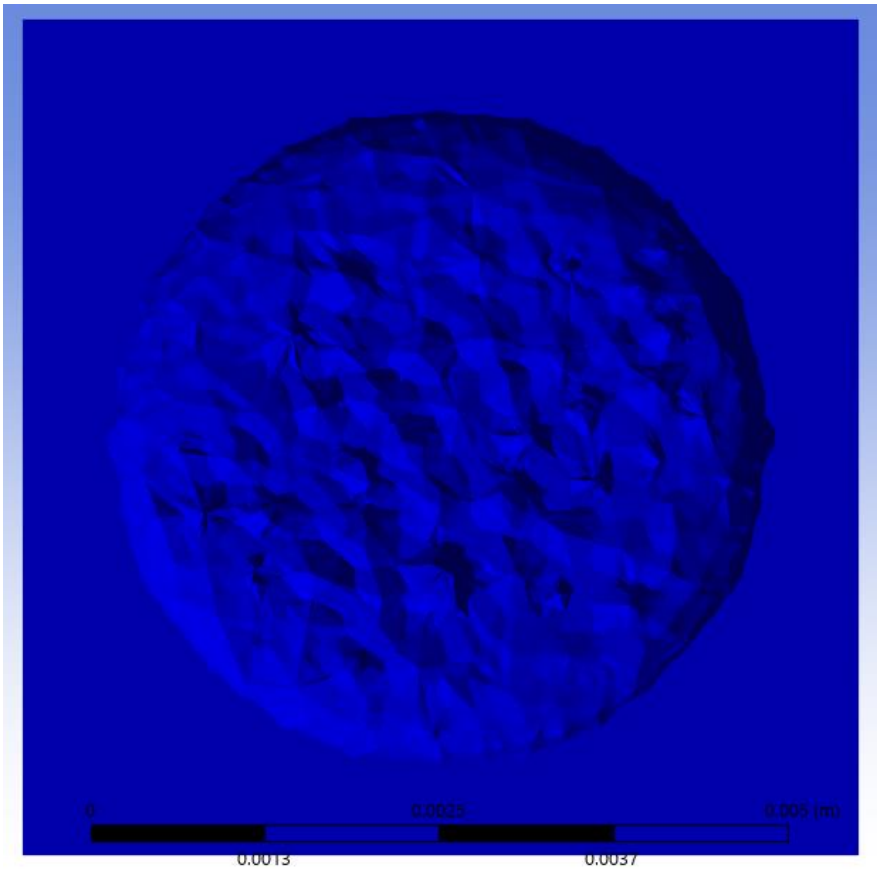

Figure 4.6: Vaporization deformation after laser impact

The qualification for vaporization deformation is when the temperature exceeds the temperature of vaporization. In this case, elements in the mesh which exceeded 4612 degrees Celsius were filtered out, leaving all elements with temperatures lower than 4612 degrees Celsius as the remaining geometry.

A similar method can be used to determine the delamination depth of the structure. By using a visual representation, the three-dimensional damage profile can be described instead of a one-dimensional delamination depth criterion. However, having the delamination depth is still useful for verifying the methods used in the finite element model. Using the glass transition temperature of 185 degrees Celsius as the damage criterion, the post-impact finite element model can be refined to remove all elements above the glass transition temperature. By removing the elements that exceed the glass transition temperature and studying the remaining geometry, the delamination depth can be determined.

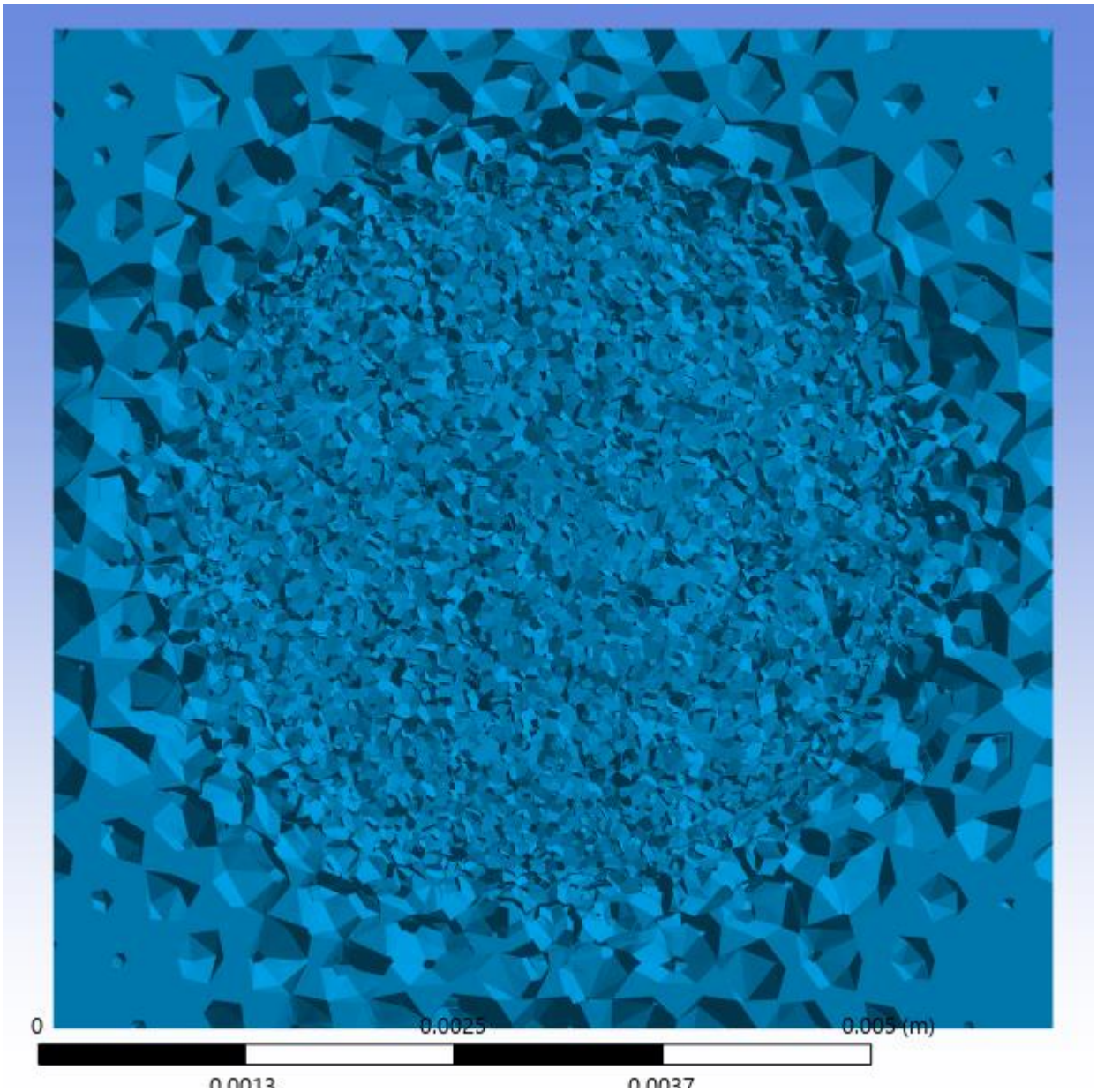

Figure 4.7: Vaporization deformation after laser impact

To note, the remaining geometry from removing elements with temperatures above the glass transition temperature is not indicative of the geometry of the deformed structure. Rather, it provides information on which parts of the target are vulnerable to delamination and epoxy damage. The delamination depth in the finite element model is slightly deeper than the experimentally found value of approximately 300 micrometers, with the delamination potentially occurring at around 600 micrometers in the finite element model. One possible explanation can be that in the experimental setup, the matrix reached glass transition temperatures in that region, but delamination did not occur. Another explanation can be due to the meshing method, which had triangular elements. Triangular elements are better at capturing rounder geometry, which would

be useful for capturing the round vaporization geometry of the deformed surface. However, the methodology for removing elements from the presentation takes the temperature of the entire mesh element into account, thus having some small imperfections due to the mesh element size. Refining the mesh to have smaller elements would help solve the issue partially, but the current model reaches the maximum mesh limit set by ANSYS.

5. Damage Prediction Case Studies

5.1 Case Study for Multiple Laser Impacts

5.1.1 Setup and Methodology

With modifications made to the original heat flux model, it is possible to study the effects of multiple laser impacts onto the same target surface. This can be useful to study, as it allows for the relation between individual damage distributions to be observed within the target surface. The original model was developed for a single laser impact in the center of the target geometry with T800 carbon fiber plies and M21 epoxy. In this case study, the model was changed to have three impacts onto various areas on the target geometry, but still on the same surface and applied in the same direction.

To apply multiple laser impacts, the geometry of the target surface was changed within ANSYS Discovery, using the single impact model as a starting point for the multiple impact model. The target surface dimensions of the single impact model were 6 millimeters by 6 millimeters, with the laser impact having a diameter of 4 millimeters. To incorporate an additional two laser impacts onto the target surface, the dimensions of the target surface must be increased. The dimensions of the target surface square were increased to 12 millimeters on each side, quadrupling the area. Noting that the depth of the laser impact damage did not reach the back surface in the previous version of the model, the depth was halved to 3 millimeters to save computational time. Using the original impact as a starting point, another laser impact was placed 2 millimeters away, with a third laser impact being placed 1 millimeter. With varying distances between the laser impact locations, the interface between different impacts can be studied, as well as the minimum required distance between impacts to result in a merged damage zone.

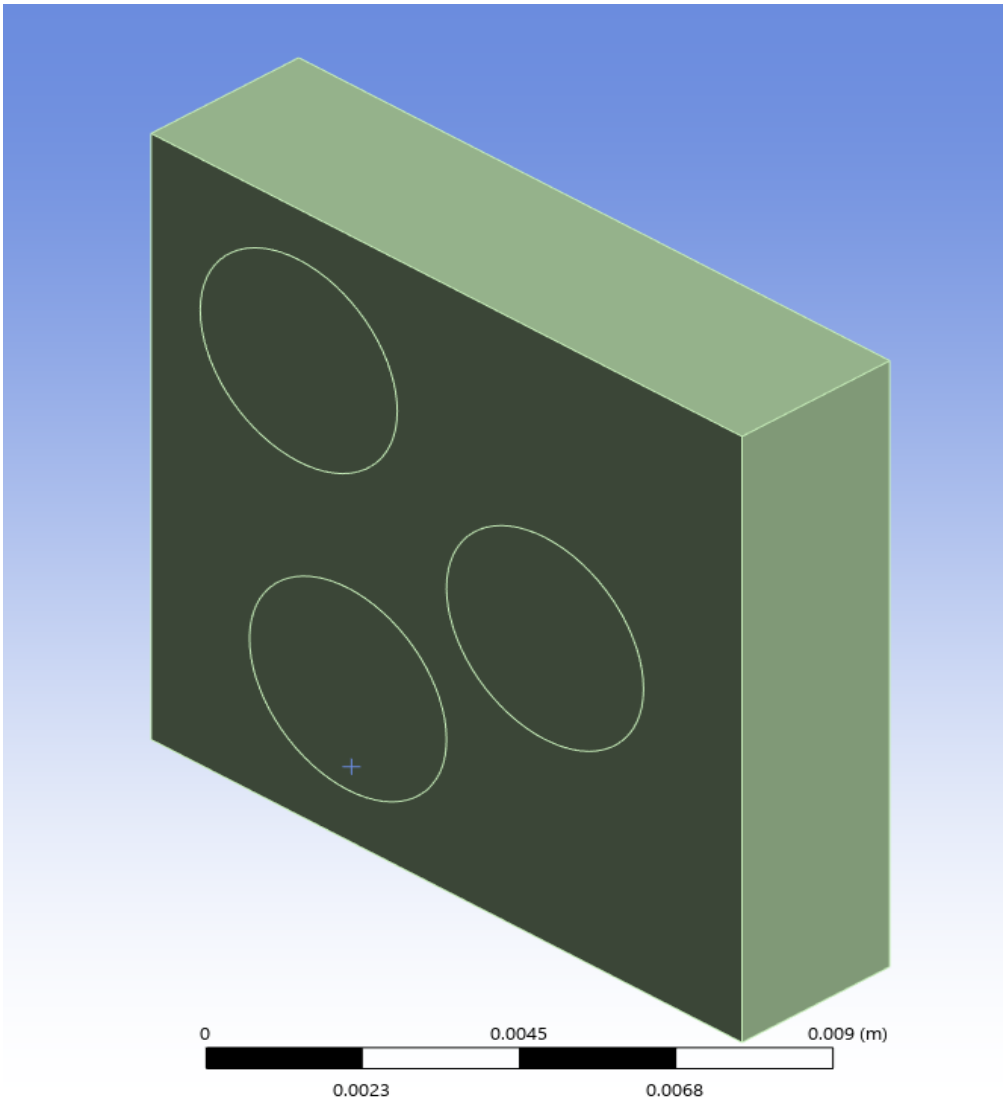

Figure 5.1: Adjusted geometry with three laser impacts

During the meshing process, it was important to maintain the same meshing rules for all three laser impacts. A face sizing with an element size of 90 micrometers was applied to all three laser impact zones. The rest of the geometry was meshed with a coarser mesh to save computational power and to stay within the element limit of ANSYS Student, as these areas were of less concern.

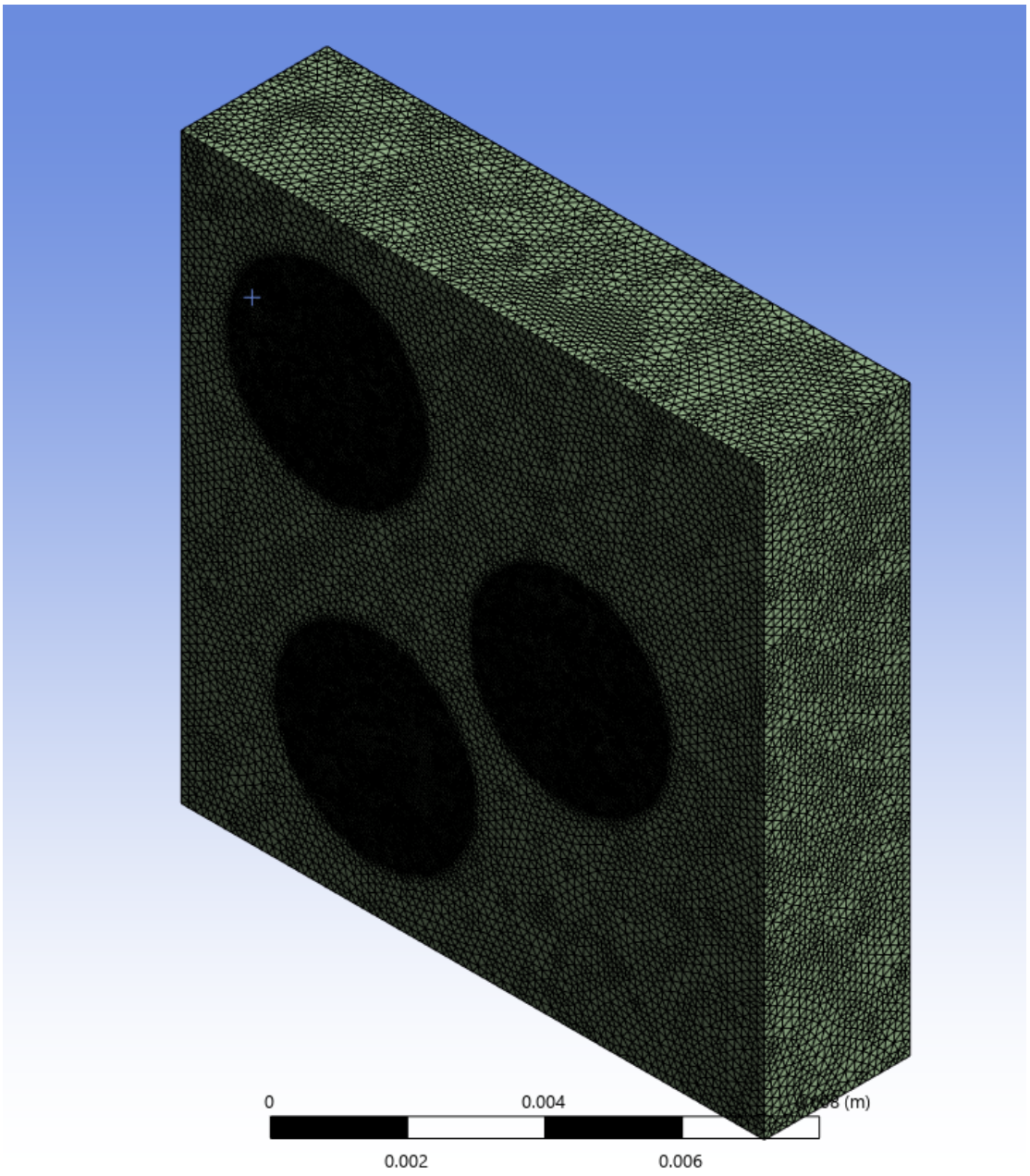

Figure 5.2: Mesh for the multiple impact model

Whenever possible, the parameters for the multiple impact model would be kept the same as the single impact model. For the multiple impact model, the initial ambient temperature was kept the same at 30 degrees Celsius. This was applied as a convection boundary condition to the target geometry. The laser was simulated using a heat flux boundary condition with properties defined in Table 5.1, identical to the properties in the single impact model:

Table 5.1: Laser shock wave properties

Intensity	Focal Radius	Pulse Time
3.43 $\boldsymbol{GW/cm^2}$	2 mm	30 ns

5.1.2 Results and Discussion

To determine damage from the laser impacts, the same method from the previous model would be used. Two different damage categorizations would be studied: vaporization damage and delamination. Vaporization damage would be categorized from the elements that exceeded the vaporization temperature of the material, which would be 4612 degrees Celsius in the case of T800 carbon fiber. Delamination would occur when the temperature of the material exceeds the glass transition temperature of epoxy, which would be 185 degrees Celsius in this case.

For vaporization damage, all elements exceeding the vaporization temperature were visually removed from the model. The vaporization damage is shown in Figure 5.3:

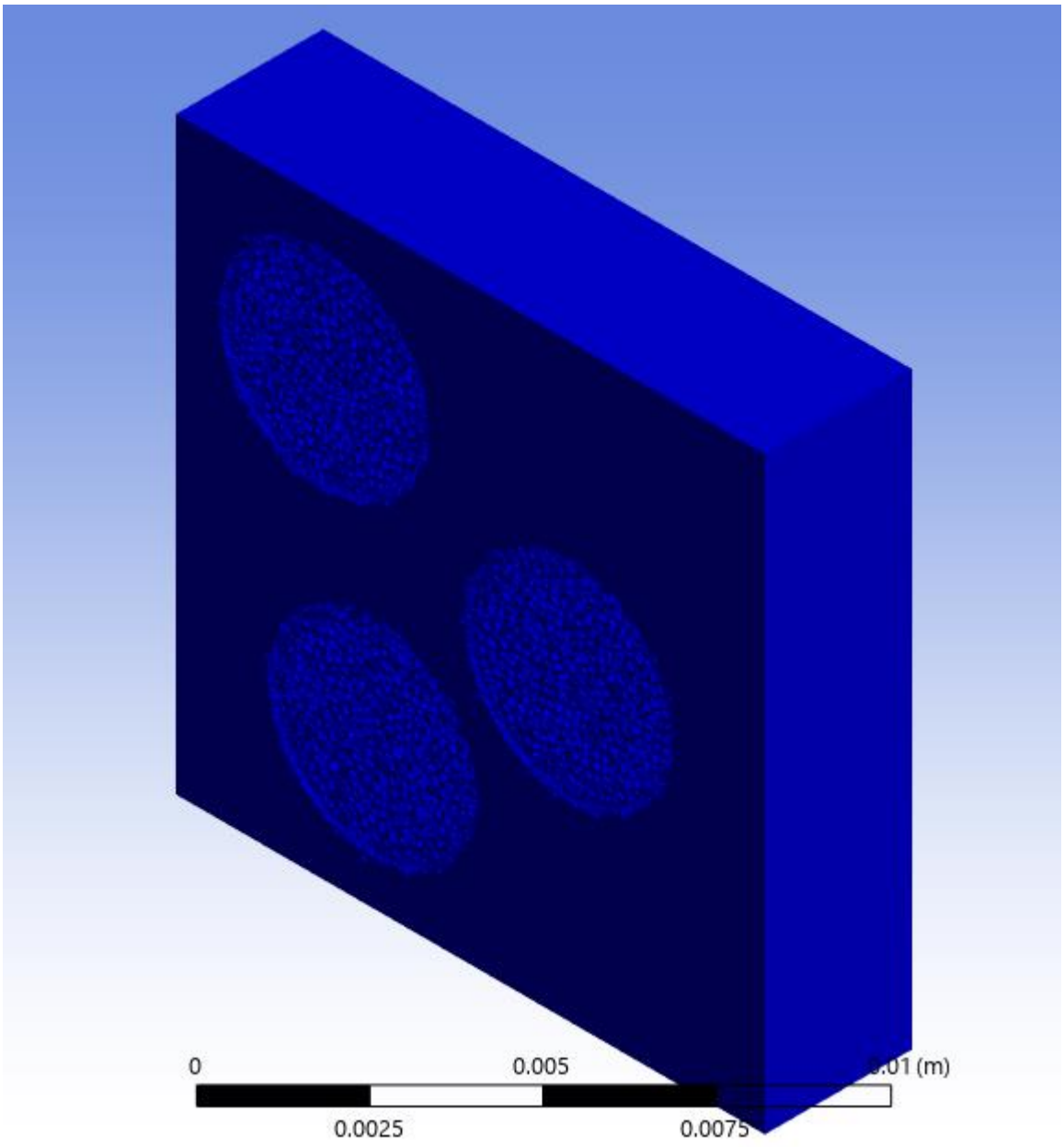

Figure 5.3: Vaporization damage for the multiple impact model

A close-up view of one of the laser impacts is shown in Figure 5.4. All three impacts behave similarly in vaporization.

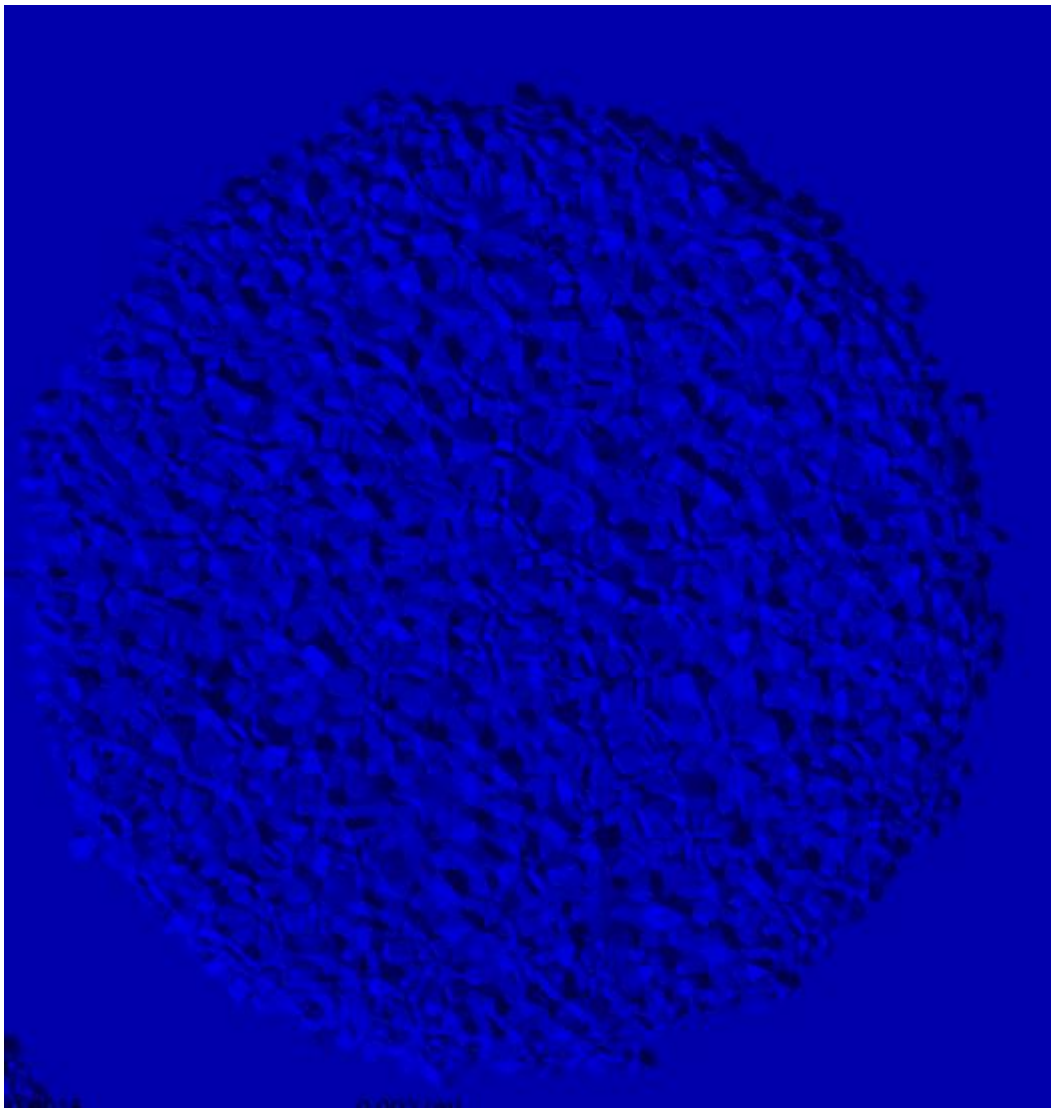

Figure 5.4: Close-up view of the vaporization damage profile

The delamination zones were obtained by changing the damage threshold from the vaporization temperature of 4612 degrees Celsius to the glass transition temperature of 185 degrees Celsius. As expected, the damage zones increased with more elements being visually removed from the model.

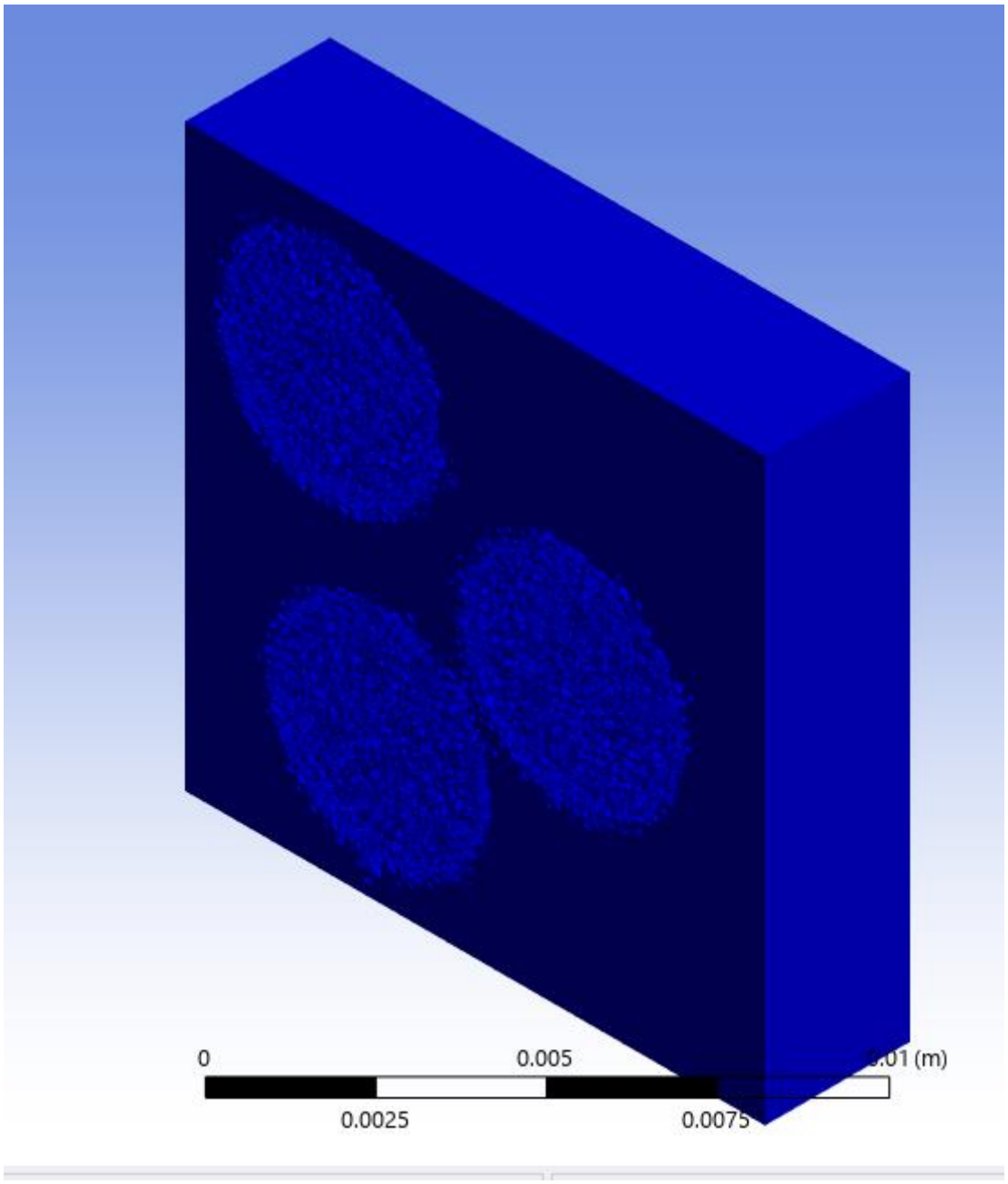

Figure 5.5: Delamination damage zones for the multiple impact model

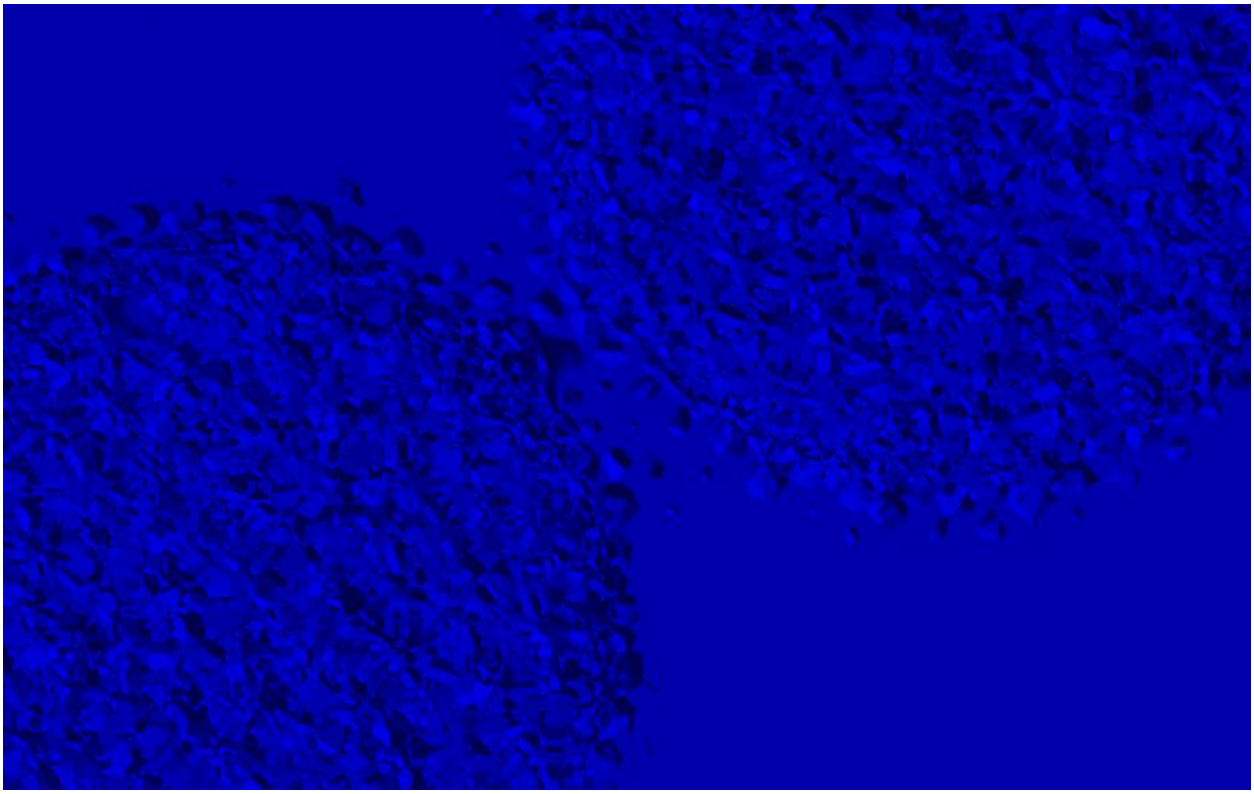

Figure 5.6: Close-up of second and third impact zones

As shown in Figure 5.6, the delamination damage zones are shown on the target surface. With the initial laser impacts being one millimeter apart from the closest edge, there is only a marginal distance between the damaged sections, showing that the damage zone extends by almost 0.5 millimeters from the original impact. To have merging damage zones occur on the target surface, several parameters could be changed. Firstly, the heat applied to the target surface can be increased. This can be done by directly increasing the heat flux value, increasing the radius of the impact, or increasing the amount of time that the laser impacts the surface. All three of these would increase the radius of the damage zone. Another option which maintains the laser profile applied would be to move the laser impacts closer together, which would require greater precision.

5.2 Case Study for Varying Epoxy Types

With the verification of the model by replicating previous study results, the finite element model can be used to study the behavior of various composite materials and epoxy types. To categorize damage, the depth of delamination method from Chapter 4 is used. The delamination is observed in the laminate when the temperature exceeds the glass transition temperature used by the epoxy. Note that this damage assumption can only be made for composite laminates, where

the epoxy material has different material properties from the laminate ply material. For an isotropic material, the vaporization temperature method can be applied to the finite element model to determine the greatest depth of damage.

Within ANSYS, the results can be analyzed to show elements within a specified temperature. To show the damage profile, the temperature results can be filtered by removing all elements below the epoxy glass transition temperature, leaving the damaged shape of elements with temperature greater than the glass transition temperature. Similarly, the result of the target surface can be obtained by filtering all elements with temperature greater than the glass transition temperature. The remaining elements would not be the visually deformed target surface, but it describes the region of the target surface where delamination does not occur.

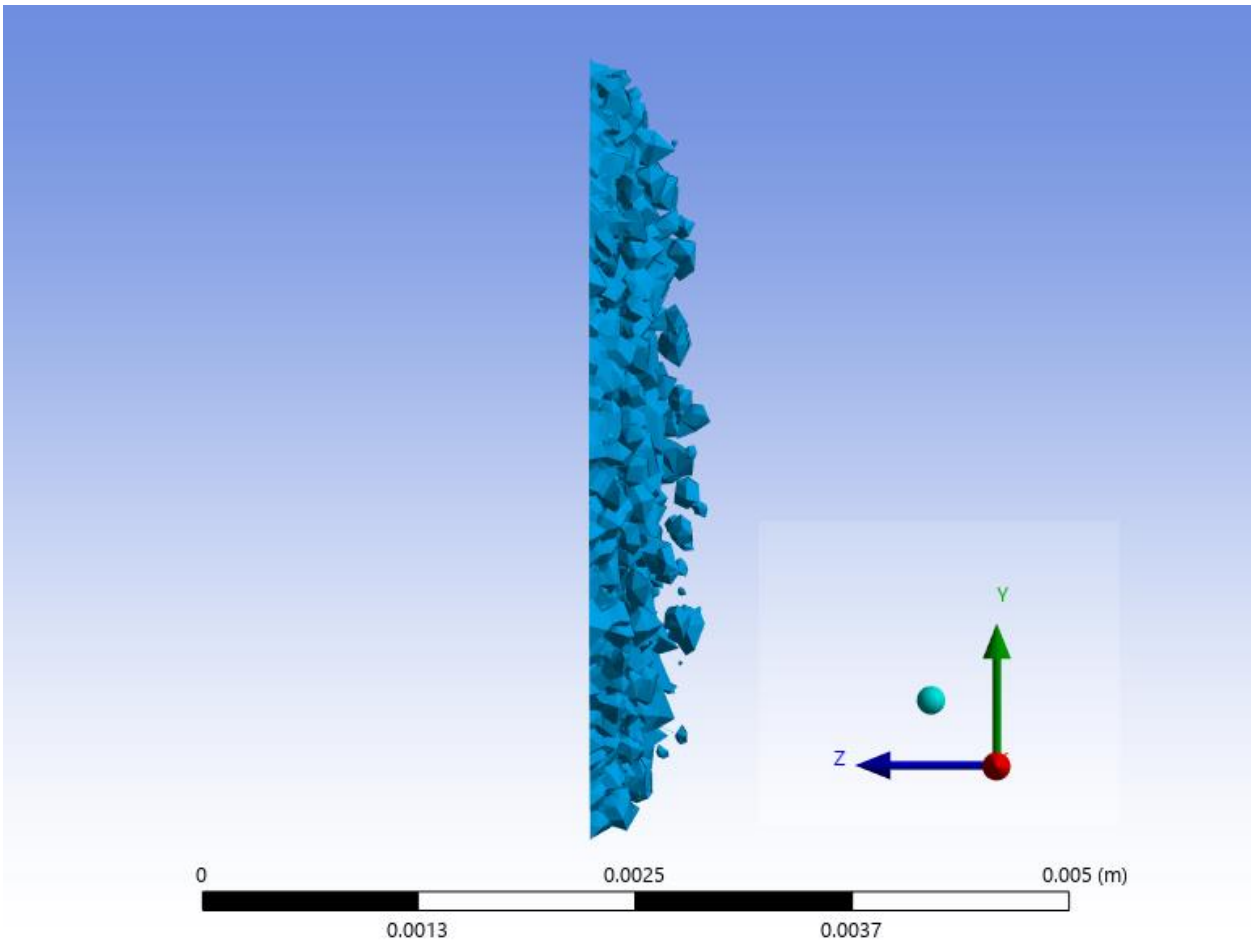

Figure 5.7: Damage representation from temperature results

The depth of delamination can be studied for T800/M21 carbon fiber, the material previously studied in the model verification. T800 carbon fiber is often used in aerospace structures, especially in primary structures [22]. As the skin is the outermost layer of aircraft, the skin is most likely to be a target surface for laser weapons. Thus, the depth of delamination should be studied with respect to realistic aircraft skin conditions in flight. Aircraft skin

thickness is generally around 2 millimeters. The previous model used in the verification process had a depth of 6 millimeters. Since the back face deformation method is not easily performed using finite element software, the model depth can remain at 6 millimeters for the purpose of this model. By doing so, the effects of laser damage on thicker depth structures can also be studied.

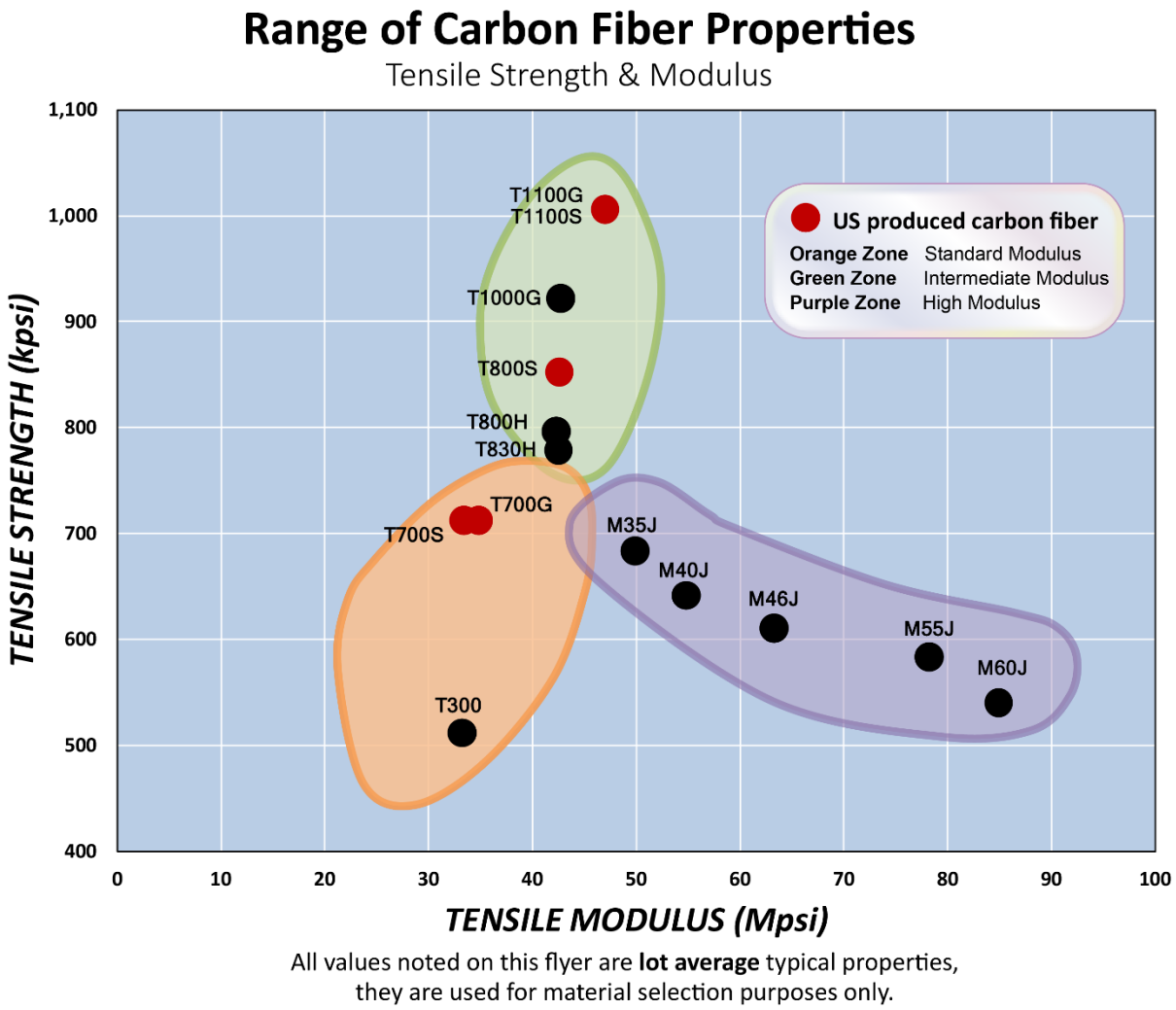

Figure 5.8: Common carbon fiber types used in aircraft [23].

For T800/M21 carbon fiber, a laser with focal radius of 2 millimeters was applied with varying heat flux. The results are graphed on a logarithmic scale with damage until a depth of approximately 4 millimeters. The results are shown in Figure 5.9:

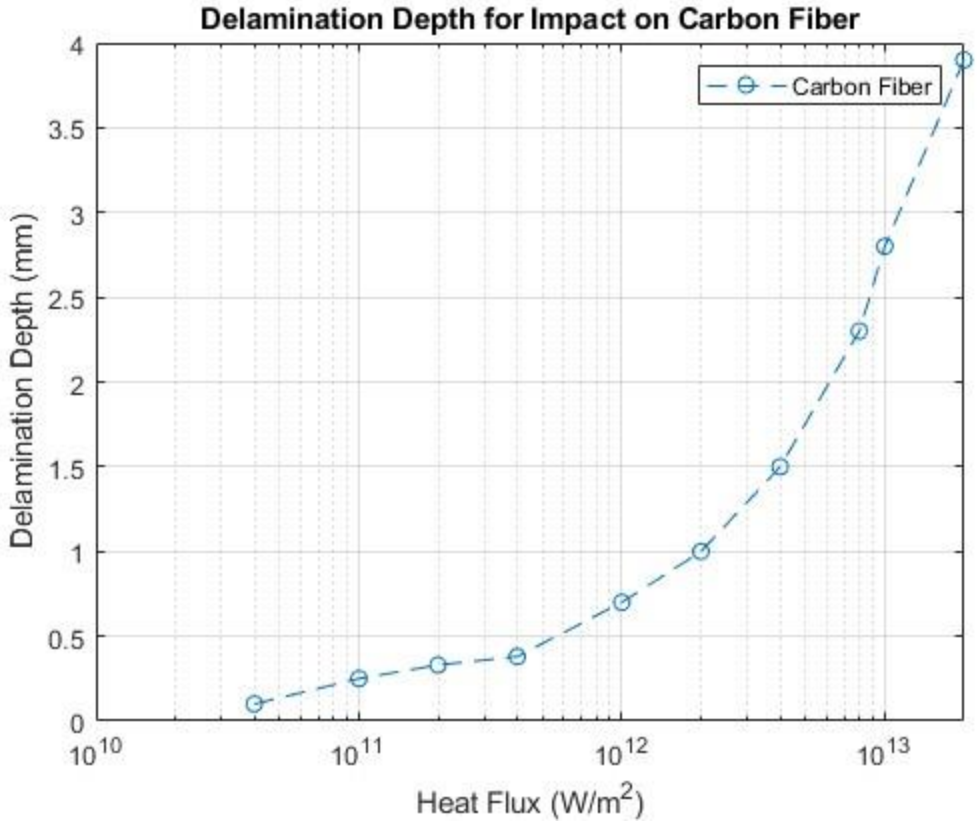

Figure 5.9: Delamination depth for impact on T800/M21 carbon fiber

The experiment was repeated for E-glass fiber, another type of composite material used in aerospace applications. The results were plotted on the same logarithmic scale as the carbon fiber for comparison.

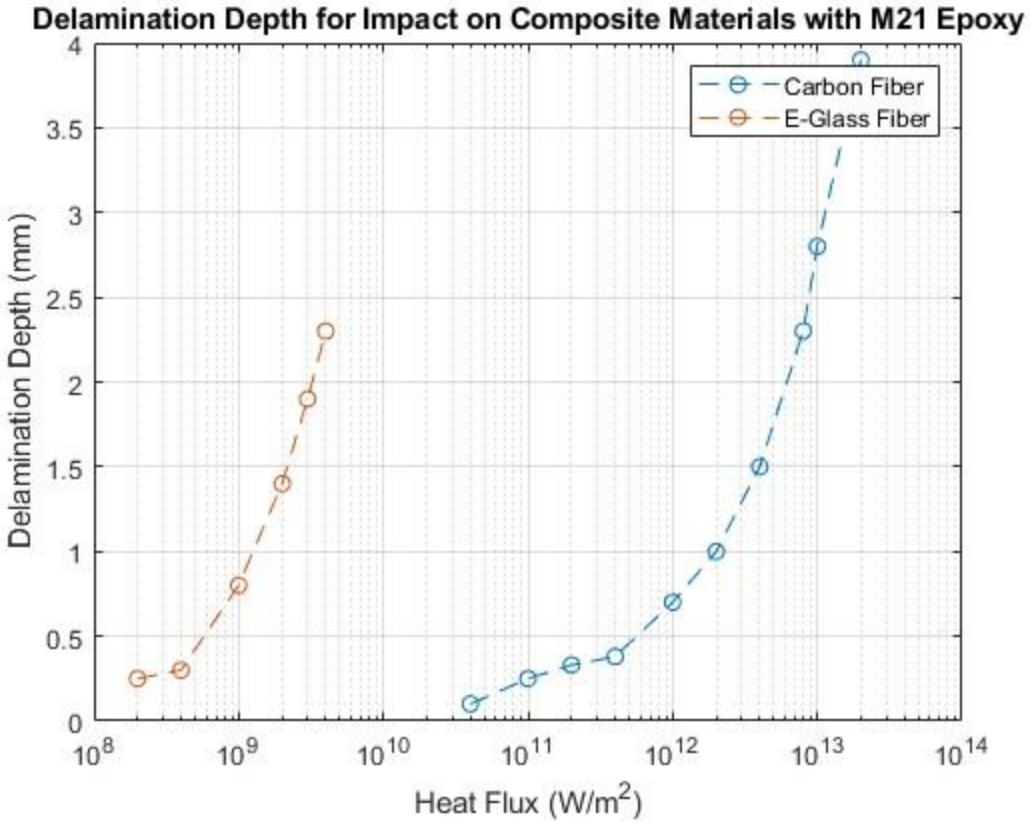

Figure 5.10: Delamination comparison for carbon fiber and E-glass fiber

From the results of Figure 5.10, it can be determined that carbon fiber can withstand a more intense laser impact compared to E-glass fiber. This could be due to E-glass fiber having a smaller specific heat constant compared to carbon fiber. Lower specific heat means that the laser requires less heating to raise the temperature of the target surface, so materials with higher specific heat constants would be more resistant to laser impacts.

In these two experimental setups, the epoxy type is set as an independent variable, thus leading to the same glass transition temperature being used as the damage criteria in both cases. A case with varying epoxy types is shown in Figure 5.11, where M20 epoxy has a different glass transition temperature.

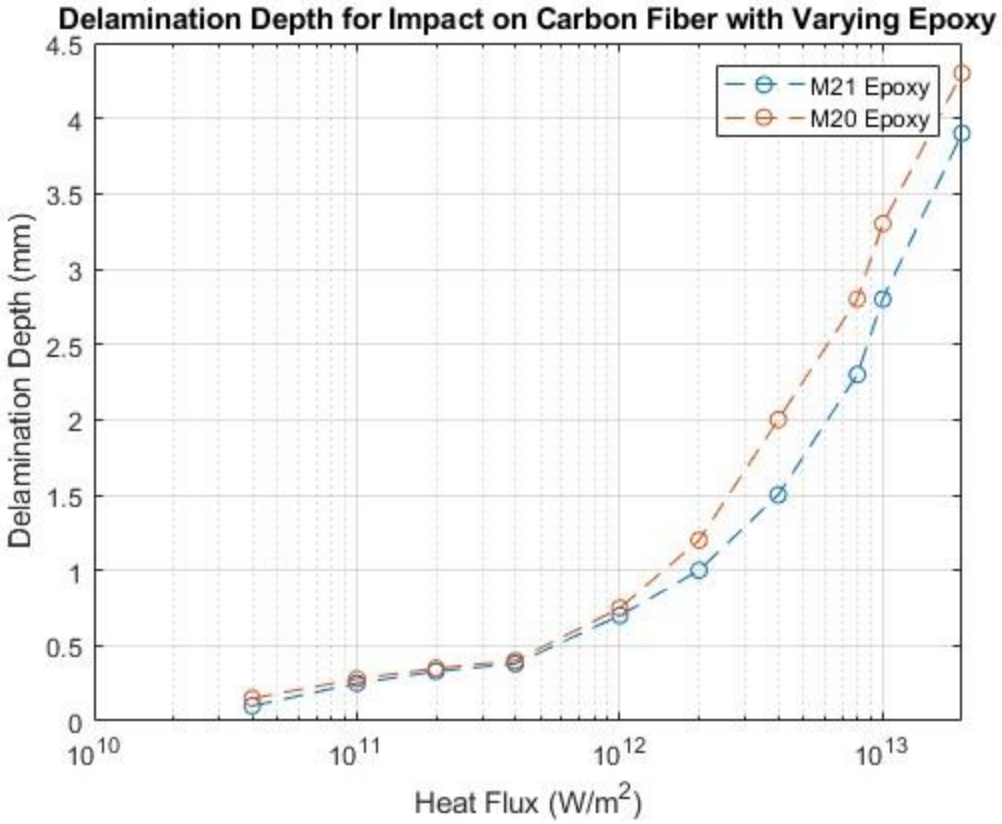

Figure 5.11: Delamination depth for varying epoxy types

6. Conclusion

6.1 Project Summary and Future Work

This project analyzed the behavior of metallic and composite structures under laser loading using a variety of models and methods for damage prediction. The first method used a MATLAB script that analyzed the ablation of a target surface by a pulsed laser. The model discretized the space into smaller elements in which temperature was approximated. The original script, developed by Zigunov, had its parameters modified to fit the desired case, resulting in a two-dimensional polar graph depicting temperature distribution with respect to distance and depth from the laser impact. Due to the radial spread of heat, heat distribution can be assumed to be the same in all transverse directions. This allowed the results to be simplified from a three-dimensional Cartesian model to a two-dimensional polar one. This simulation was performed for both a metallic and composite case, with all parameters kept the same except the thermal and material properties of the target surface. In addition, a second script was developed to analyze the effects of heat diffusion throughout the target in the time immediately after the laser impact. This part of the simulation analyzed the temperature distribution distance with respect to time after laser impact, removing all temperature values above the vaporization temperature of the material to categorize damage. Using this model, the heat would diffuse to a certain depth over the course of a few seconds, but would stabilize.

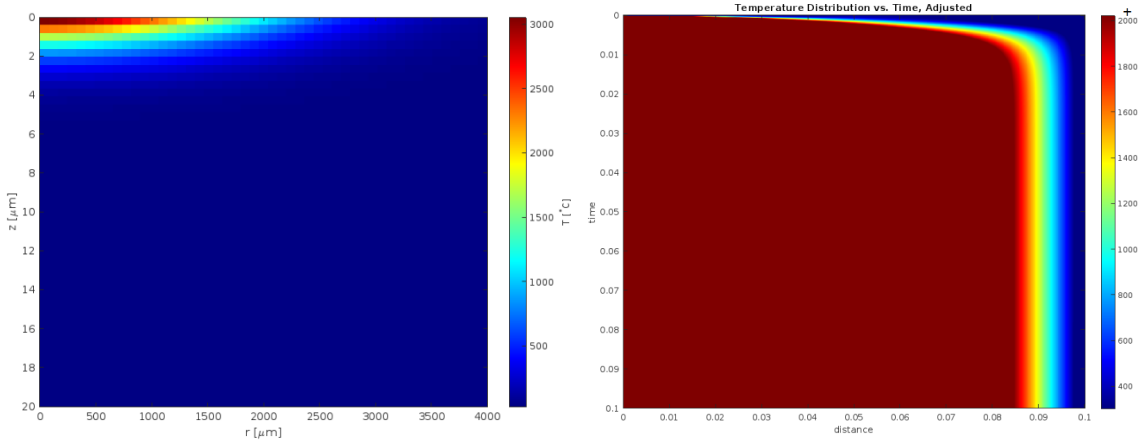

Figure 6.1: MATLAB laser simulation

The second model developed was a finite element model that represented the laser impact as a heat flux applied to the target surface. Using the transient thermal analysis module built into ANSYS, a heat flux was applied axially to the target surface face with the heat density of the applied laser. For the remaining parts of the model, a heat convection boundary condition was applied with the ambient initial temperature of the scenario. A mesh refinement study was performed with the goal of creating a grid-independent solution. To check for the validity of the

model, a case study that was performed physically was recreated using the finite element model. The case study referenced two methods of analyzing composite damage from a laser impact: back-face deformation and depth of delamination. For the finite element model, the depth of delamination, as well as the vaporization temperature, were used as the damage criteria. Comparing delamination damage for the two cases resulted in a delamination depth of 300 millimeters, while the model predicted a delamination depth of approximately 600 millimeters.

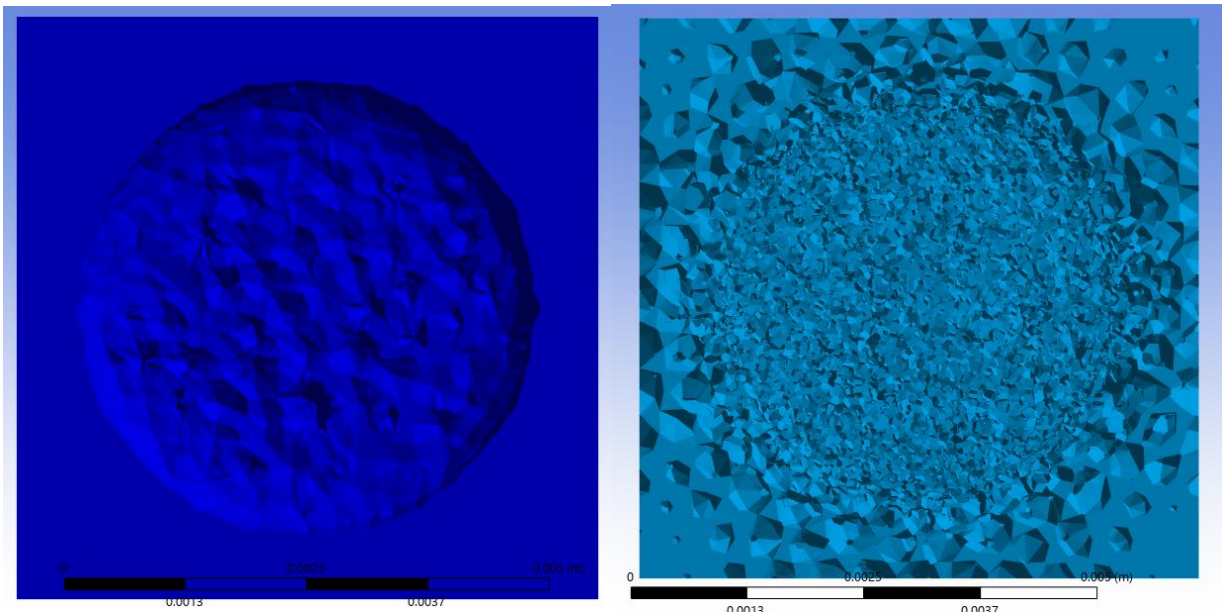

Figure 6.2: Vaporization and delamination results

With the model methodology verified with experimental results, a few more case studies were analyzed. Another version of the finite element model was developed to include multiple laser impacts and analyze the interfaces between different impact craters. In addition, a case study was performed analyzing the response to a laser impact with varying composite and epoxy types. Some future studies could include the addition of a heat diffusion study as a supplement to the heat flux finite element model, as that model only models the period where the target is impacted by the laser.

References

[1] Keller, J. “Ride of the Valkyries: The Army Is Getting the US Military’s Most Powerful Laser Weapons Yet,” *Military.com,* 12 Oct. 2023. Retrieved 24 Feb. 2024 from <https://www.military.com/daily-news/2023/10/12/ride-of-valkyries-army-getting-us-militarys-most-powerful-laser-weapons-yet.html>

[2] SMITeam. “4 Applications for Composite Technology and Materials in the Military,” *SMI Composites,* 18 Aug. 2023. Retrieved 24 Feb. 2024 from <https://www.smicomposites.com/4-applications-for-composite-technology-and-materials-in-the-military>

[3] Zhang, Y. X., Zhu, Z., Joseph, R., & Shihan, I. J. Damage to aircraft composite structures caused by directed energy system: A literature review. *Defence Technology*, *17*(4), 1269–1288, Aug. 2020.

[4] Pal, S., Gubeljak, N., Hudak, R., Lojen, G., Rajtukova, V., Brajlih, T., & Igor, D. “Evolution of the metallurgical properties of Ti-6Al-4V, produced with different laser processing parameters, at constant energy density in Selective Laser Melting,” *Results in Physics*, *17*, 103186, Jun. 2020.

[5] Wang, R., Garcia, D., Kamath, R. R., Dou, C., Ma, X., Shen, B., Choo, H., Fezzaa, K., Yu, H. Z., & Kong, Z. (James). “In situ melt pool measurements for laser powder bed fusion using multi sensing and correlation analysis,” *Scientific Reports*, *12*(1), Article 1, 12 Aug. 2022.

[6] Shepelev, V. V., Inogamov, N. A., & Fortova, S. V “Thermal and dynamic effects of laser irradiation of thin metal films,” *Optical and Quantum Electronics*, *52*(2), 88, 29 Jan. 2010.

[7] Ecault, R., Boustie, M., Touchard, F., Pons, F., Berthe, L., Chocinski-Arnault, L., Ehrhart, B., & Bockenheimer, C. “A study of composite material damage induced by laser shock waves,” *Composites Part A: Applied Science and Manufacturing*, *53*, 54–64, Oct. 2013.

[8] Lazov, L., Angelov, N., Draganov, I., Atanasov, A., Lengerov, A., Teirumnieks, E., & Balchev, I. “Finite element modeling of laser aluminum marking,” *Journal of Physics: Conference Series*, *1859*(1), 1 Jan. 2017. https://doi.org/10.1088/1742-6596/1859/1/012017

[9] Zigunov, F. “Laser ablation heat transfer simulation.” 23 Aug. 2023. Retrieved 24 Feb. 2024 from <https://www.mathworks.com/matlabcentral/fileexchange/134237-laser-ablation-heat-transfer-simulation>.

[10] Li, Y., Lin, C., Murengami, B., Tang, C., & Chen, X”. Analyses and Research on a Model for Effective Thermal Conductivity of Laser-Clad Composite Materials,” *Materials*, *16*, 7360, 27 Nov. 2023.

[11] Fu, G., Zhang, D., He, A., Mao, Z., & Zhang, K. “Finite element analysis of interaction of laser beam with material in laser metal powder bed fusion process,” *Materials, 2018, 765, 10* May 2018.

[12] “Carbon Fiber,” *American Elements.* Retrieved 24 Feb. 2024 from <https://www.americanelements.com/carbon-fiber-7440-44-0>.

[13] Cook, P. S., & Ritchie, D. J. “Determining the laser absorptivity of Ti-6Al-4V during laser powder bed fusion by calibrated melt pool simulation,” *Optics & Laser Technology*, *162*, 109247, Jul. 2023.

[14] Boley, C., & Rubenchik, A. “Modeling of laser interactions with composite materials,” *Applied Optics, 52,* 3329–3337, 7 May 2013.
[15] Alsaddah, M., Khan, A., Groom, K., & Mumtaz, K. “Use of 450-808 nm diode lasers for efficient energy absorption during powder bed fusion of Ti6Al4V,” *The International Journal of Advanced Manufacturing Technology, 113,* 1–20, 21 Feb. 2021.
[16] Caywood, W. C., Rivello, R. M., & Weckesser, L. B. “Tactical Missile Structures and Materials Technology.” *Johns Hopkins APL Technical Digest,* Sep. 1983.
[17] LeVeque, R.J. “Finite Difference Methods for Ordinary and Partial Differential Equations,” *Society for Industrial and Applied Mathematics,* 2007.
[18] Zeneli, M., Nikolopoulos, A., Karellas, S., & Nikolopoulos, N. “Chapter 7—Numerical methods for solid-liquid phase-change problems,” *Ultra-High Temperature Thermal Energy Storage, Transfer and Conversion* (pp. 165–199), 2021.
[19] “Finite Difference Approximating Derivatives—Python Numerical Methods.” *Python Programming and Numerical Methods, 20,* 27 Nov. 2020.
[20] Abdullah, M.S., Abdullah, A.S., & Samad, Z. “Defects in holes-making on composite panels: A review on delamination,” *Hole-Making and Drilling Technology for Composites,* 2, 17-30, 2019.
[21] “Explaining the Glass Transition Temperature,” *Mallard Creek Polymers.* Retrieved 8 Nov. 2024 from
< https://www.mcpolymers.com/library/understanding-the-glasstransition-temperature>
[22] “Hexcel HexPly M21 Curing Epoxy Matrix,” *MatWeb.* Retrieved 9 Nov. 2024 from
<https://www.matweb.com/search/datasheet.aspx?matguid=50512b22a4b84334b177966a2469f736&ckck=1 >
[23] “Carbon Fiber Material,” *Rpproto.com.* Retrieved 8 Nov. 2024 from
< https://www.rpproto.com/carbon-fiber-material>.